CHALMERS

Design, implementation, and evaluation of vehicle control systems using a side slip estimator

Master's thesis in Automotive Engineering

MEET RAKHOLIA
OSCAR TISELL

Department of Mechanics and Maritime Sciences
CHALMERS UNIVERSITY OF TECHNOLOGY
Göteborg, Sweden 2019

MASTER'S THESIS IN AUTOMOTIVE ENGINEERING

Design, implementation, and evaluation of vehicle control systems using a side slip estimator

MEET RAKHOLIA
OSCAR TISELL

Department of Mechanics and Maritime Sciences

Division of Vehicle Engineering and Autonomous Systems

CHALMERS UNIVERSITY OF TECHNOLOGY

Göteborg, Sweden 2019

Design, implementation, and evaluation of vehicle control systems using a side slip estimator
MEET RAKHOLIA
OSCAR TISELL

Master's thesis 2019:10
Department of Mechanics and Maritime Sciences
Division of Vehicle Engineering and Autonomous Systems
Chalmers University of Technology
SE-412 96 Göteborg
Sweden
Telephone: +46 (0)31-772 1000

Chalmers Reproservice
Göteborg, Sweden 2019

Design, implementation, and evaluation of vehicle control systems using a side slip estimator
Master's thesis in Automotive Engineering
MEET RAKHOLIA
OSCAR TISELL
Department of Mechanics and Maritime Sciences
Division of Vehicle Engineering and Autonomous Systems
Chalmers University of Technology

Abstract

Vehicle control systems have been integral to the performance and stability of a vehicle. In this thesis, two vehicle control strategies namely, the *yaw controller* and the *yaw–beta controller*, were presented. The control algorithm was based on the *model predictive control* method. A simulation environment developed using a two track *vehicle model* coupled with a tire model based on the *magic tire formula* was used to test the controllers in different test scenarios. These tests were carried out to evaluate the performance of the two controllers with respect to performance and stability. The results showed small differences between the performance of the controllers, but enough to indicate the initial assumptions on the behaviour. The yaw–beta controller was more stable than the yaw controller at the expense of the vehicle performance. However, the results did not show significant enough differences to determine the magnitude of any potential gains.

Keywords: model predictive control, vehicle model, yaw controller, yaw–beta controller, magic tire formula

Acknowledgements

We would like to thank Ola Benderuis for providing support and guidance during the master thesis.

A special gratitude goes to the *Chalmers Formula Student Driverless* team for providing us with an opportunity to work with vehicle control systems.

Thesis advisor: Ola Benderius

Thesis examiner: Ola Benderius

Contents

1 Introduction

The vehicle used for *Chalmers formula student driverless* is an electric vehicle with two 40 kW motors driving the rear wheels. Each motor is coupled to one wheel and is independent of the other. This provides a unique opportunity to implement a torque distribution system which can generate desired vehicle yaw moment to achieve a desired vehicle handling. The system can be used to maintain the yaw stability as well as to increase the vehicle handing capabilities in difficult manoeuvres. The independent torque control also makes it possible to regulate torque to each wheel to eliminate unwanted slip between the wheel and the ground.

In this thesis, a torque vectoring and slip control system have been designed and implemented to investigate whether this will increase longitudinal and lateral control of the vehicle. The thesis evaluates the performance change caused by implementing a body side slip angle. The validation of the thesis is limited to the vehicle used by the Chalmers formula student driverless team. The vehicle is equipped to be driven autonomously, which will be used for the evaluation of the stability systems.

The scope of the thesis was to develop a vehicle control system that can generate a desired vehicle orientation for a desired vehicle speed. Two different systems for torque vectoring are compared to show the difference in performance. Where the two systems differ, is that one will try to make use of a body side slip. The ratio between lateral and longitudinal velocities, which is the body side slip, is one of the states used to approximate the tire forces. As side slip is not easily measurable in most vehicles, it becomes an important problem to find a solution for. The systems are simulated using a two-track *vehicle model* to achieve a first iteration of parameters used in the controllers. The simulation results are then used to compare the performance of the two systems.

Beyond implementing a yaw rate controller the project also includes the creation of a longitudinal slip controller. The vehicle used for testing is a rear wheel driven car. On vehicles with only one driven axle it is practical to measure the longitudinal slip. This is due to slip being a result of applied torque on the wheel, hence the front axle can be assumed to have zero slip. Thus, by comparing the front wheel speed to rear wheel speed, slip on the rear wheels is determined. This information is used to design a controller that penalises wheels rotating faster than the front wheels.

1.1 Problem statement

The Formula student competition is an engineering and a racing event. Hence, the focus is on the performance of the vehicle. For a driverless vehicle the performance means completing the track with maximum accuracy in minimum time. The accuracy of the path following depends on the orientation of the vehicle and the time required to complete the track depends on the vehicle speed. Therefore, a vehicle control system is required which can generate a desired orientation at desired speed. To conclude, the problem statement of this thesis is as follows.

> *How does the performance of a formula student race car change with a side slip angle estimator?*

The performance of the control systems, within this thesis, is defined as:

Lap time The better system will produce a faster lap time. Hence, a low lap time is an indication of a high performing system.

Rise time Time taken for the yaw rate to change from a specified value, to another. This is a measurement of the control systems response time.

Overshoot The amount of exceeded yaw rate relative the reference after a step-response. A good controller design will minimise overshoots.

Positional deviation from path The ability of the control to follow the reference, which is also the desired outcome.

Body side slip Low body side slip limits the tire side slip which increases stability. The peak body side slip of each manoeuvre is used for comparison. Given that the track drive is not a singular manoeuvre, the standard deviation as well as the root mean squared (RMS) values of the body side slips will be considered.

1.2 Limitations

The project development has been limited to the formula student vehicle and has been tailored to facilitate the Formula student rules. The system has been validated in an environment similar to the one used at the competition shown in Figure 3.18.

2 Theory

This section will present a background on existing knowledge in the field of vehicle control. The background for the thesis is divided into four sections. The first section includes a driver model and path generation. The second section describes different possibilities for control systems implemented on vehicles. The third section includes side slip estimation. The last section covers test scenarios for validating the results. The scenarios were selected such that it resembles actual field tests to improve validity and tuning of the system.

2.1 Driver model and path generation

The driver model used is a module that provides reference values for the longitudinal and lateral motion of the vehicle. The lateral reference is in terms of yaw rate required and the longitudinal reference is in terms of acceleration required. In previous work [1] a feedback model was used based on the yaw rate error to calculate the desired steering angle for the vehicle. In one study [2], a Fuzzy logic was used for the lateral and longitudinal driver model. It used a preview point approach to follow a given track. A similar method is adopted here as well, where the preview point controls the lateral offset of the vehicle form the track. An article [3] explained a neural network based driver model which was trained with actual driver data. This model used the velocity estimation based on the path curvature, which is similar to the approach adopted here.

2.2 Control system

The vehicle control system described here consists of a plant and a controller. The plant is a physical model of the system being controlled. Hence, a vehicle model is required. There are two types of vehicle models in general, the one track (bicycle) model and the two track model. The bicycle model assumes the vehicle only has one wheel per axle, which is approximated in the center-line of the vehicle. The model has 3 degrees of freedom: longitudinal translation, lateral translation and rotation around vertical axis. Many studies related to vehicle control [4], [5] use the bicycle model as a plant for the vehicle control system. This model is simple and requires less computational power. On the other hand, a two track model considers two wheels on each axle and hence incorporates the load transfer mechanism. This mechanism can be used to study the vehicle handling characteristics during a turn. This model can be represented using 7, 8 or 14 degrees of freedom model depending on the motions considered. The difference between aforementioned types of vehicle models has been explained in a previous study [6]. Some studies related to vehicle control uses [7], [8] a two track vehicle model with 7 degrees of freedom. There are other studies [9], [10] that also uses a 8 degrees of freedom model. A complex 14 degrees of freedom model is used in a study [11] for simulation and validation of vehicle control system. It can be seen that a two track model provides a better approximation of the actual vehicle as compared to the one track model but is computation heavy. As the controller is to be used in the real time, a simple model will be much more effective. Similar argument can be made for a 14 degree of freedom model which being computation intensive, makes it less suitable for real time use whereas a 3 degree of freedom model requires much less computational power and can satisfactorily describe the vehicle motion. Hence a one track vehicle model with 3 degrees of freedom was chosen as a plant for the current vehicle control system.

The orientation of the vehicle is a consequence of the steering angle and the torque distribution on the rear wheels. The desired rate of change of orientation, yaw rate, can be obtained form the path to be followed. Hence, a reference yaw rate is generated from the bicycle model and compared to the current yaw rate of the vehicle. Depending on the difference in the compared quantities a controlled output is generated. This output is the steering angle and the torque distribution. Also, an arbitration model is developed to determine the percentage of yaw rate generated by steering action and by the torque distribution.

The 7 degrees of freedom model is a non linear model. A variety of control algorithm exists that can be used for the purpose of yaw rate control. A comparision between a PID controller with anti windup and a sliding mode controller (SMC) was shown in a study [5]. The simulation results shows that a linear controller like PID with use of anti wind up strategy can produce similar lateral characteristics to SMC for a brake in turn manoeuvre. One of the study [12] uses a SMC controller along with Karush–Kuhn–Tucker (KKT) optimiser to control the vehicle yaw rate. The controller shows promising lateral behaviour and also significant reduction in use of brakes as compared to ESC system. A fuzzy logic based yaw control is implemented and simulated in the previous work [13]. The result shows that the fuzzy logic controller is able to handle the nonlinearities of the vehicle model and provides satisfactory results in limit cornering conditions. An optimal guaranteed cost coordination controller (OGCC) is compared to an optimal coordination (OC) based on linear quadratic regulator (LQR) in a previous study [9]. The OGCC control model used also takes into account the uncertainty in the tire cornering stiffness. Simulation shows that OGCC is slightly better than OC in dry conditions, but the OGCC performs much better in split μ and low μ conditions for slalom and double lane change manoeuvres. The results for a LQR yaw rate controller coupled with a slip controller is reported in an article [14]. It is one of the few cases in the literature that validates the control model via field test.

For the purpose of this thesis a *model predictive controller* (MPC) has been used to control the yaw rate of the vehicle. As the driverless vehicle is equipped with a camera and a LIDAR, it provides a unique opportunity to obtain future track information. This allows for a future reference generation which can be used by an MPC to calculate a suitable current optimal input.

Furthermore, a state observer is implemented in the control module which fuses the plant output with the actual output measured by the vehicle sensors, to provide with a better estimate of the vehicle states. This makes one track vehicle model more feasible despite it being a poor representation of the actual vehicle.

2.3 Side slip estimation

The body side slip (β) is the angular difference between the vehicle's longitudinal direction and velocity. Measurement of β practically includes many challenges and the sensors that can measure it are quite expensive. Hence, for conventional vehicles, only way to estimate β is by combining data from various vehicle sensor and running them through estimators. In a study [15], GPS and IMU data are used to estimate body side slip. It can be seen that the estimation highly depends on the accuracy of GPS measurement and noise level of the IMU measurements. An IMU based β estimation for skid steered robot using an extended Kalman filter is explained in a previous work [16]. The experimental validation shows an improved lateral behaviour by using estimated value of β. A novel method of β estimation via vision for mobile robots on sandy terrain is proposed in a study [17]. This method traces the wheel track print on the sand via images from the camera and estimates the resultant velocity direction. By comparing the resultant velocity direction and the heading direction β can be calculated.

As the formula student vehicle being used has camera and LIDAR for detecting cones, a vision based β estimation can be developed. A vision based system would directly perceive vehicle motion and hence would not require complicated models for predicting the vehicle motion.

2.4 Test scenarios

Validation of the controller behaviour highly depends on the test scenarios selected. The aim of the test scenarios should be to prove the controller behaviour at limit conditions. A variety of test scenarios exists for the purpose of evaluating the vehicle handling behaviour. In one of the study [18] various test scenarios used for vehicle testing are discussed.

Steady state cornering The vehicle drives in a circle with either constant radius, speed or steering angle. The test reveals information about the vehicle's under- and oversteering properties. It is not a suitable test for benchmarking electronic control systems (ECS) since there are very few dynamic effects being tested.

Sine with dwell The vehicle is driven at constant velocity, and a sine wave of one period is introduced as steering input. At the second peak, a dwell is introduced for 500 ms, followed by finalizing the sine wave. This manoeuvre is commonly used when testing ECS system.

Double lane change The vehicle changes lane within 13.5 meters, continues in the lane for 11 meters and turns back to the original lane. The lanes are three meters wide, and are off-set by 4 meters (center to center). The double lane change and sine wave tests are similar and assesses the same vehicle and ECS qualities.

Step input A steer step input is given to the vehicle. This test is used to relate the lateral acceleration with steering input. The main output from this test is the transient response of the vehicle.

Braking with split coefficient of friction The vehicle brakes with different surfaces for left and right side. For conventional vehicles this is a valuable test to perform, but the vehicle of this study is expected to run in a controlled environment where split friction is unlikely to occur.

Continuous sinusoidal input A continuous sinusoidal steering input is given to the vehicle. This test is mainly used to perform a frequency analysis of the vehicle.

3 Methodology

This section will present background on existing knowledge in the field of vehicle control as well as the methods being used to answer the question posed by this thesis. The thesis is based on simulations, and validation of said simulations. Firstly, an introduction to the simulation is presented. This section explains specific implementation decisions, as well as the general structure. The following sections describe various models used to simulate the physical vehicle, and how to generate inputs for simulation. This includes generating a reference for controlling lateral and longitudinal position, tire-road contact models, load transfer, aerodynamic effects as well as equations of motion.

Subsequently, the control strategies for making the vehicle follow the correct path is given. Two different versions are presented which utilise information regarding the surroundings in separate ways. One trying to control for lowest possible body side slip which is why a subsection of how to estimating the body side slip also exists.

3.1 Simulation setup

This section explains the information flow and parameter specifications of the simulation aspect of this thesis. A more in depth explanation of specific models or functions is provided after this section. The simulation was performed in discrete time steps, with a fixed sample time. The remainder of this section will describe the information flow and arbitration of one time step. In Figure 3.1 a visualisation of the information flow is shown.

The main input, and where the information flow starts, to the simulation is a 2D-map for the vehicle to follow. The map is a list of coordinates, without any specific spacing. The map is used by the driver model, and after comparing with the vehicle's position, points in front of the vehicle are selected. These points are passed on as the local path, and are transformed to the vehicle's coordinate frame. The driver model calculates a yaw rate and acceleration reference for the vehicle. This information is passed on to a longitudinal and a lateral control system.

From here on, the lateral and longitudinal information take parallel paths, and are treated independently. The longitudinal control system converts the acceleration request to a torque request which is sent to the electric motor model. The motor model simulates the output of the motor based on restrictions and the torque request. The motor is limited by maximum torque and a maximum torque rate. The motor torque is used in the longitudinal tire model which models the rotational position of the wheels which is used for finding the longitudinal tire forces.

Tire forces are calculated using a semi-empirical model based on tire slip. To find the slip of the tires the velocity of the vehicle is compared to the rotational velocity of the tires. Therefore, there is a necessity to model the motion of the wheels. The angular acceleration of the wheels is calculated using equations of motions. The acceleration is then numerically

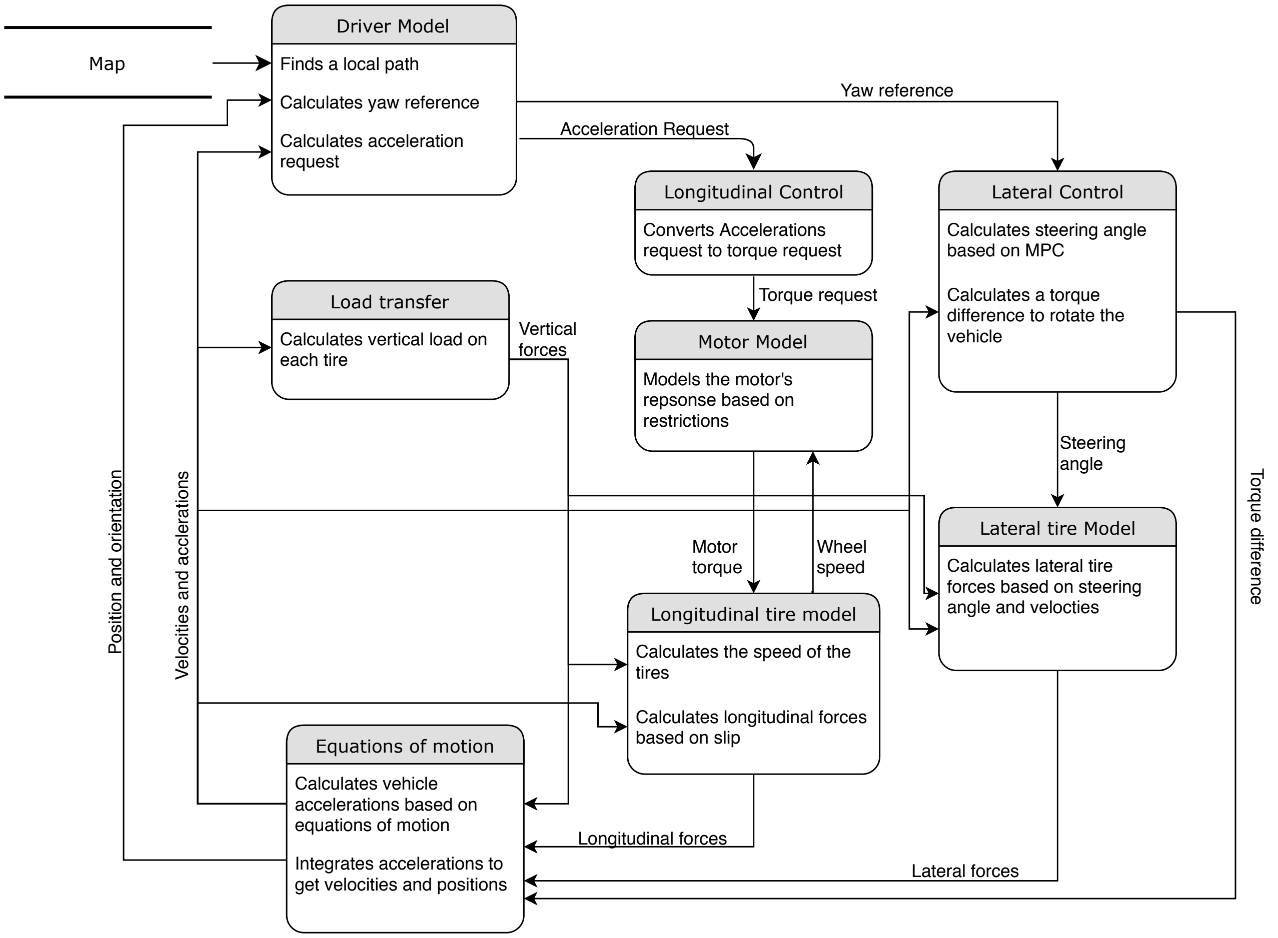

Figure 3.1: *Flow chart of the simulation process including what information is sent to which modules.*

integrated using Euler method to calculate the wheel's velocity for the next time step.

An MPC controller is used for lateral control. It is a model based controller where the reference yaw rate or reference side slip is used to calculate an optimum steering input. The steering angle calculated is the wheel angle. This method can be extended to calculate an optimum torque differential for torque vectoring. This control system uses a state observer to predict a better state by using the model and measurement.

The lateral tire forces are taken from a lookup table, based on the tire slip angles. The slip angles will depend on the kinematic state of the vehicle and the steering angle. The lookup table contains measurement data mapping side slip and vertical load to lateral force for the tires used on the vehicle. The vertical load on the tire will affect the friction between the tire and road. Hence, vertical load is also necessary to calculate lateral force. This true for tire forces in longitudinal direction as well.

The information about vertical load is taken from a load transfer model. When determining the load transfer the roll, though not the pitch effects, are considered. Only load shift due to accelerations are regarded. Apart from load transfer, aerodynamic effects also increase the force on the wheels. The aerodynamic forces depend on the velocity of the vehicle, and is therefore necessary, along with accelerations, to calculate the vertical load of the vehicle.

With lateral and longitudinal forces on the tires known, as well as any aerodynamic forces, all the external forces on the vehicle are known. Accelerations on the vehicle, including yaw acceleration, are calculated using Newton's equations. The accelerations are integrated numerically using Euler's method, resulting in the velocity and position of the vehicle. The assumption made for this to be true is accelerations being constant between time steps.

3.2 Path generation and driver model

To supply the vehicle with inputs, a driver model is needed. The model is sent a map containing coordinates of a path to follow. In a real vehicle, these coordinates are produced by a perceptive system. In the simulation the perceptive system was assumed to have perfect performance and the path to follow was taken from predefined track, referred to as the global map. To simulate the perceptive system, all points on the global map which are in a conical area in front of the car were defined as the local map. The local map is what the car is expected to see in a real environment. When executing its task, the local map is what the driver model will have access to. The driver model has two main functions to fulfil. To provide input to the longitudinal and lateral control systems, such that the vehicle follows the given path.

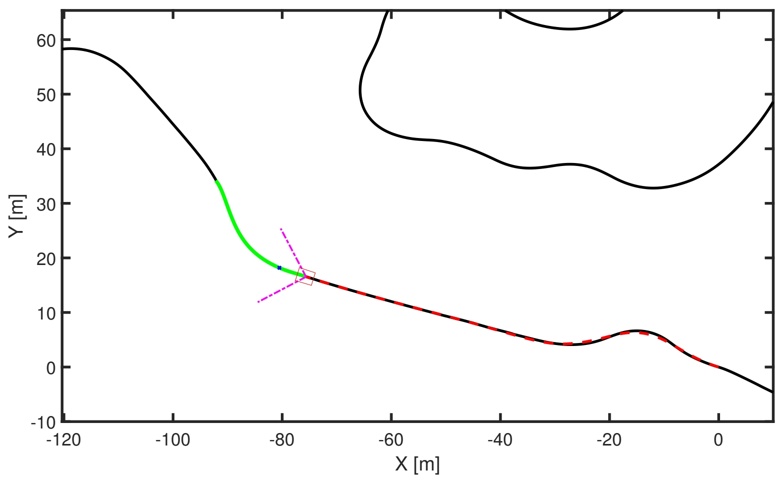

Figure 3.2: *Local map and global map for track drive simulation*

Figure 3.2 shows the global map and local map in the same plot. The black solid line is the global map and the green solid line is the local map. The two dashed magenta lines are the field of view lines. This field of view describes the angular region within which the vehicle looks for a local path. The dashed red line shows the path taken by the vehicle. The small blue point in the front of the vehicle is the Aim point. The direction of the vector from vehicle to the aim point is the desired heading direction.

3.2.1 Lateral reference

The lateral control system requires future yaw rate as reference. It is the driver model's purpose to supply that reference. This is achieved by first approximating the local path as a polynomial function, using polynomial regression. If $(\boldsymbol{x}, \boldsymbol{y})$ are the set of points making up the local path, then $\boldsymbol{y}$ can be approximated as

$$\boldsymbol{y} \approx \boldsymbol{X}\boldsymbol{p}, \qquad \begin{aligned} \boldsymbol{X} &= [1,\, \boldsymbol{x},\, \boldsymbol{x}^2 \,...,\, \boldsymbol{x}^n] \\ \boldsymbol{p} &= [p_0,\, p_1,\, ...,\, p_n]^T \end{aligned}$$

This method works well unless the local track turns more than 90°, due to the inherent restrictions of a polynomial. For the polynomial $y(x)$ there can only be one value of y for a any given x. If the track turns more than 90° this condition is violated, and it will not be possible to describe the path with a polynomial. However, note that the track will always be oriented to the vehicle's coordinate frame, and if the track turns more than 90° relative to the vehicle heading, it is like outside its perceptive area.

The polynomial coefficients, $\boldsymbol{p}$, are estimated using ordinary least squares method. This method finds the $\boldsymbol{p}$ which minimises the residual between the curve and the points squared. Eq. (3.1) calculates $\boldsymbol{p}$ using ordinary least squares method.

$$\boldsymbol{p} = (\boldsymbol{X}^T\boldsymbol{X})^{-1}\boldsymbol{X}^T\boldsymbol{y} \tag{3.1}$$

As mentioned, the control system requires a yaw rate reference as input. The curve radius and the yaw rate relate according to

$$\dot{\Psi} = \frac{v_x}{R} \tag{3.2}$$

To calculate the yaw rate reference, the vehicle's velocity throughout the path is needed. Hence, a prediction regarding the future velocity is made, which assumes it to be constant. Secondly, the curve radius has to be estimated. Using the track's curvature to create a reference is equivalent to asking the car to drive with the same change in direction as the track. It performs well as long as the car stays on track, but cannot compensate if an offset occurs, since there is no dependency on the vehicle's position relative to the track. To have a reference which is also dependent on the vehicle's position relative to the track, an aim point based method is used.

A point is selected on the local path. The point is selected to be at a distance away from the vehicle which is equal to the vehicle's speed multiplied with a time constant. By assuming the vehicle will approach this point in a perfect circle arc, with constant speed as mentioned, the yaw rate can be calculated according to Eq. (3.2). To find the radius of the arc the angle to the center theorem is used [19]. The arc theorem concludes the arc angle being twice the angle between the vehicle's heading and the aim point. Since the coordinates of the aim point are known the distance to the vehicle is also known. The ceneter of the arc, the vehicle and the aim point forms an isosceles triangle with one side length known and one angle. Figure 3.3 shows a geometrical representation of the arc and the triangle.

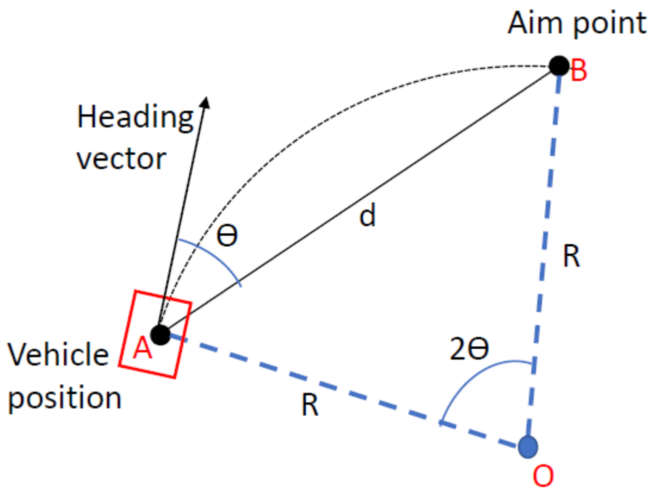

Figure 3.3: *Circle arc connecting the vehicle with an aim point. R is used to estimate the curve radius of the path.*

From the triangle in Figure 3.3, the radius is calculated using law of cosines according to

$$d^2 = 2R^2 - 2Rcos(2\theta) \tag{3.3}$$

$$R = \frac{d}{\sqrt{2(1 - cos(2\theta))}} \tag{3.4}$$

Once the curvature of the path is known, a yaw rate reference can be found using Eq. (3.2).

3.2.2 Longitudinal reference

The longitudinal control reference used is an acceleration request. The acceleration request is based on the curvature of the track. With coefficients $\boldsymbol{p}$, a function $y(x) = [1, x, ..., x^n]\boldsymbol{p}$ is defined, which is an approximation of the local track. The curve radius of function $y(x)$ can be calculated as a function of x according to

$$R(x) = \frac{\left(1 + (\frac{dy}{dx})^2\right)^{2/3}}{||\frac{d^2y}{dx^2}||} \tag{3.5}$$

Points on the local map are assigned a curvature based on the polynomial path, which gives a discrete track mapped with corresponding curvature. An initial estimate of the velocity profile is made, based on maximum lateral acceleration, $a_{\text{y,max}}$. The lateral acceleration of the car is equal to $\frac{v^2}{R}$, which gives the velocity profile $v(x) = \sqrt{a_{\text{y,max}} R(x)}$. A body following this velocity profile will experience the lateral acceleration limit throughout the path, except when the path is perfectly straight. The velocity profile is considered a *candidate* velocity profile, meaning it is a first estimate which will later change.

As mentioned, following this profile will lead to maximum lateral acceleration at all times, and no available force in longitudinal direction due to friction limitations. The required longitudinal acceleration to follow the velocity profile is examined by back-tracing the path, point by point and calculating the resulting acceleration. If the total acceleration at point n on the path is higher than the limit, the velocity candidate for points n and $n-1$ is set to the lowest of the two velocities. Until the total acceleration is lower than the limit at all points, the process is repeated. Once this is achieved the candidate velocity profile is considered the actual velocity profile, and a longitudinal acceleration reference can be create by differentiation.

Only the acceleration reference closest in time is used to control the motor, the rest of the profile is created only to ensure that a feasible future path and velocity profile exists. The motor is, however, based on torques and not vehicle acceleration. Hence, a conversion to motor torque is required. The net force in longitudinal direction is estimated to

$$F = m(a_r + g\, f_r) + \frac{1}{2} C_d A \rho v^2 \tag{3.6}$$

The first term, ma_r is the inertial force to accelerate the vehicle, and a_r is the requested acceleration. The second term $mg\, f_r$ is an approximation of the rolling resistance. A rubber tire is soft, and when rolling it deforms, causing a power loss. This approximation assumes the loss is proportional to the weight of vehicle, with f_r as a rolling resistance coefficient. The last term is to overcome the aerodynamic drag cause by the vehicle, where C_d is the drag coefficient, A is the frontal area of the vehicle and ρ is the density of air. This force will have a moment on the wheel equal to

$$T = F\, R_w = (m(a_r + g\, f_r) + \frac{1}{2} C_d A \rho v^2)\; R_w \tag{3.7}$$

with R_w being the wheel radius.

To find the appropriate motor torque, T is divided by the gear ratio. Which, finally, gives the torque request to send to the motors.

3.3 Vehicle model

The model used is a two track vehicle model with 8 degrees of freedom, and is described in the following section. The purpose of this model is to simulate the response of a vehicle, and more specifically CFS17's car. This vehicle is to be used to validate the results of the simulation. Hence the vehicle model used in the simulation is made to behave as similar as possible to the CFS17 car.

3.3.1 Equations of motion

In Figure 3.4, v_x and v_y are the longitudinal and lateral velocities respectively. The angular rotation around the vertical axis passing through the center of gravity is denoted r. The steering angle is shown as δ and α are slip angles. Slip is defined as the angular difference between the vehicle's (or tire's) longitudinal orientation and the direction of the velocity for said part.

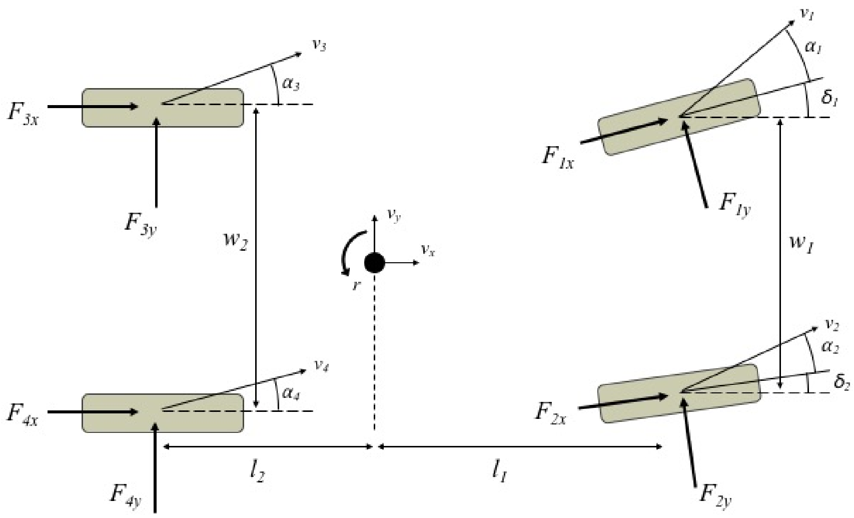

Figure 3.4: *Free body diagram of a four wheel vehicle with front wheel steering.*

Force equilibrium from Figure 3.4 results in the following equations:

$$ma_x = m(\dot{v}_x - rv_y) = F_{1x}cos(\delta_1) + F_{2x}cos(\delta_2) - F_{1y}sin(\delta_1) - F_{2y}sin(\delta_2) + F_{3x} + F_{4x} - \frac{1}{2}C_d A \rho v_x^2 - mg\, f_r \tag{3.8}$$

The last two terms represent the aerodynamic drag and rolling resistance, under the assumption that the vehicle is always travelling forward.

$$ma_y = m(\dot{v}_y + rv_x) = F_{1x}sin(\delta_1) + F_{2x}sin(\delta_2) + F_{1y}cos(\delta_1) + F_{2y}cos(\delta_2) + F_{3y} + F_{4y} \tag{3.9}$$

From moment equilibrium, the following equation is found:

$$\begin{aligned} I_z\dot{r} = (F_{1x}cos(\delta_1) - F_{2x}cos(\delta_2) - F_{1y}sin(\delta_1) - F_{2y}sin(\delta_2))\frac{w_1}{2} + (F_{3x} - F_{4x})\frac{w_2}{2} + \\ (F_{1x}sin(\delta_1) + F_{2x}sin(\delta_2) + F_{1y}cos(\delta_1) + F_{2y})cos(\delta_2))l_1 - (F_{3y} + F_{4y})l_2 \end{aligned} \tag{3.10}$$

Geometric compatibility constrains on the vehicle gives the following equations:

$$\begin{aligned} \alpha_1 &= \delta_1 - \arctan\left(\frac{v_y + rl_1}{v_x - r\frac{w_1}{2}}\right) & \alpha_2 &= \delta_2 - \arctan\left(\frac{v_y + rl_1}{v_x + r\frac{w_1}{2}}\right) \\ \alpha_3 &= -\arctan\left(\frac{v_y - rl_1}{v_x + r\frac{w_1}{2}}\right) & \alpha_4 &= -\arctan\left(\frac{v_y - rl_1}{v_x - r\frac{w_1}{2}}\right) \end{aligned} \tag{3.11}$$

3.3.2 Tire model

Lastly, a relation between the wheel kinematics and forces is necessary. For the specific vehicle used in this study, measurements between tire slip and forces exists. Hence, a lookup table is used to calculate the lateral forces produced. However, there is not sufficient data to use the same method in the longitudinal direction. Instead, a semi-empirical model, similar to Pacejka's magic tire formula [20] was used, shown in Eq. (3.12).

$$F_x = \mu F_z sin(C\, atan(B\, s_x - E(B\, s_x - atan(B\, s_x)))) \tag{3.12}$$

where s_x is the longitudinal slip of the wheels and is defined as

$$s_x = \begin{cases} \frac{R_w\omega - u}{u} & \text{if } u > 0 \\ \frac{u - R_w\omega}{u} & \text{if } u < 0 \end{cases} \tag{3.13}$$

where u is the longitudinal velocity of the vehicle, ω is the rotational velocity of the wheel and R_w is the wheel radius.

The lateral force versus slip angle measurements were collected in a test rig with alternating vertical load. In Figure 3.5, the results from the measurements are show.

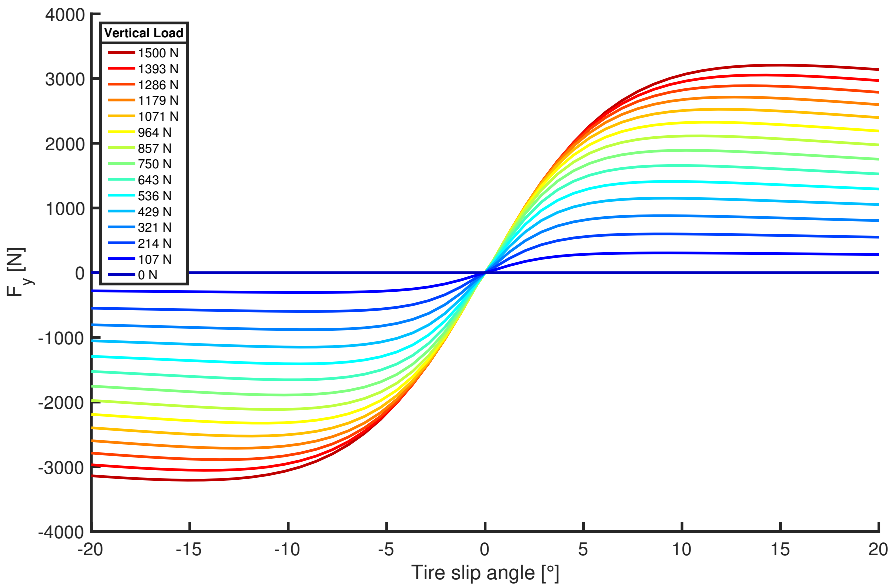

Figure 3.5: *Lateral tire forces vs slip angle, measured in test rig. The curves represent different vertical loads.*

The measurements are performed by attaching the tire to an arm equipped with force measuring units, and running it on a sand belt. The contact between the tire and driving surface in these measurements will typically have high values of friction coefficient, μ, which are not to be expected for normal driving on asphalt. In Figure 3.6, F_y/F_z is shown as a function of vertical load on the tire. To make the tire data fit the scenario which is desired in the simulation, all lateral forces in Figure 3.5 are scaled by a constant. The constant is chosen to achieve a desired friction coefficient. Figure 3.6 shows how a scaling factor is found by deciding a desired friction coefficient for a given load.

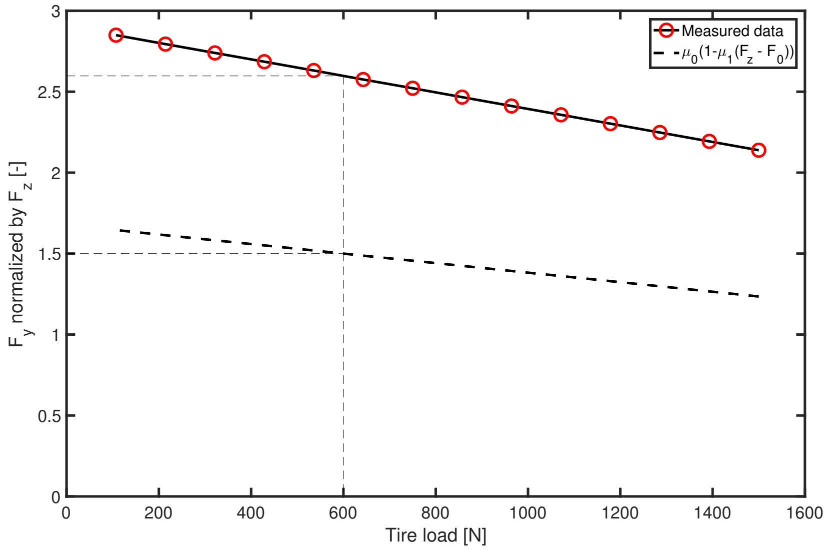

Figure 3.6: *Lateral force normalised by vertical load, shown as a function of vertical load. The dashed curve shows the expected friction in the simulation environment.*

Figure 3.6 indicates that the friction coefficient is linearly dependent on the vertical load on the tire, which was used later in this section. Measurement data from when Chalmers Formula Student's car has previously run shows lateral acceleration of up to 15 m/s^2, with an average vertical load of 600 N per wheel, see Figure 3.7. Hence, the measurement data is multiplied with a factor such that the maximum lateral force with 600 N vertical load, divided by 600 N is equal to $15/g \approx 1.5$.

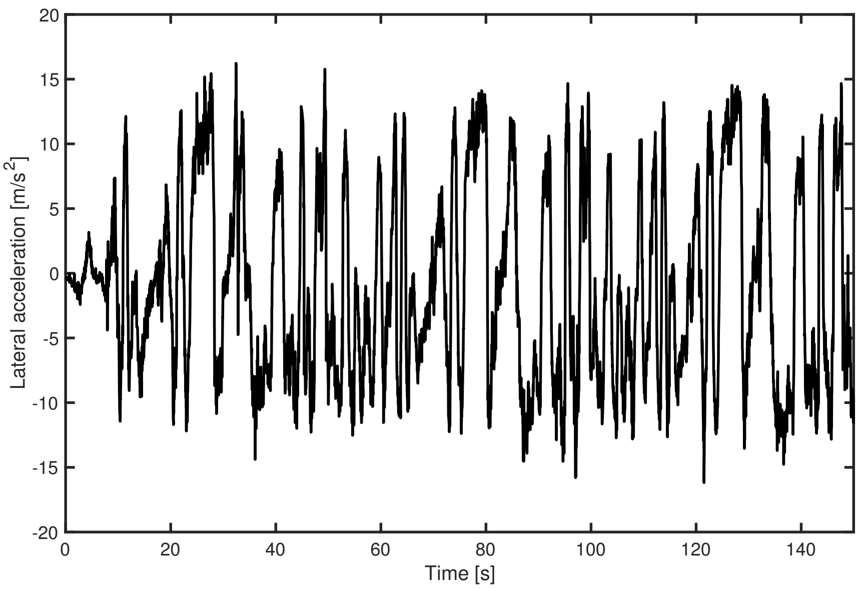

Figure 3.7: *Lateral acceleration measured on a test track with the Chalmers Formula Student race car.*

When simulating the vehicle, the friction coefficient at each tire can be calculated using the data available in Figure 3.6. Using linear regression, the the data can bit fit to the linear function (3.14).

$$\mu = \mu_0(1 - \mu_1(F_z - F_0) \tag{3.14}$$

Fz_0 is selected as the average static load on a tire, and μ_0 is known from test track measurements. μ_1 is calculated according to:

$$\mu_1 = ((F_z - F_0)^T(F_z - F_0))^{-1}(F_z - F_0)^T(\frac{\mu}{\mu_0} - 1) \tag{3.15}$$

Eq. (3.14) was used to calculate the longitudinal forces. The friction coefficient was calculated using data from lateral tire dynamics, and in this model, since data for longitudinal forces is limited, longitudinal friction coefficient is assumed to be same as lateral. The last information needed to calculate the longitudinal forces are the wheel slips, which is acquired from Eq. (3.13). To calculate the slip, the rotational velocity of the wheels needs to be modelled. The rotational velocity is modelled by integrating the rotational acceleration of the wheel.

$$I_{\text{yw}}\dot{\omega} = T_d - T_b - F_x R_w \tag{3.16}$$

I_{yw} is the rotational inertia of the wheels, T_d is a driving torque, T_b is a braking torque and F_x is the tire-road friction force.

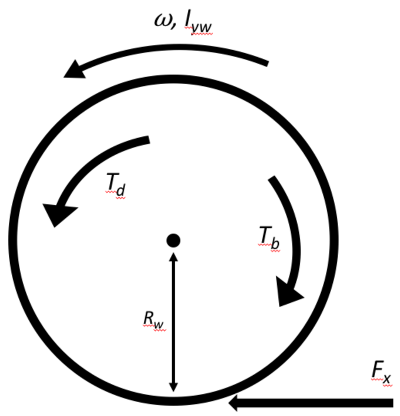

Figure 3.8: *Rotational force and torque diagram of a wheel.*

The rotational speed of the wheels is found by integrating $\dot{\omega}$. In a discrete simulation the driving and braking torque are used as the inputs to the vehicle model, and ω is calculated as

$$\omega(t + \Delta t) = \omega(t) + \frac{T_d - T_b - F_x(t)R_w}{I_{\text{yw}}}\Delta t \tag{3.17}$$

where Δt is the time step.

3.3.3 Load transfer

When a vehicle is moving, vertical load is shifted between the wheels. Modelling this load transfer correctly is important, due to tire forces being highly dependent on the vertical load. The model used when simulating is based on the assumption that roll dynamics are in steady state, and without any pitch dynamics. Roll being in steady state implies the roll angle ϕ's derivatives being zero. For most vehicles, ϕ typically has low range, at least relative to the sample time used for the simulation, meaning that $\ddot{\phi} = 0$ is an acceptable assumption. For a vehicle in steady state, the roll angle is calculated according to

$$c_\phi \phi = m_s a_y h_0 cos(\phi) + m_s g h_0 sin(\phi) \tag{3.18}$$

if small angles for ϕ is assumed, the equation can be written as

$$\phi = \frac{m_s h_0}{c_\phi - m_s h_0 g} a_y \tag{3.19}$$

where h_0 is center of gravity's height above the roll axis and m_s is the vehicle's sprung mass. c_ϕ is the roll stiffness of the vehicle. Figure 3.9 displays a free body diagram of the vehicle rolling.

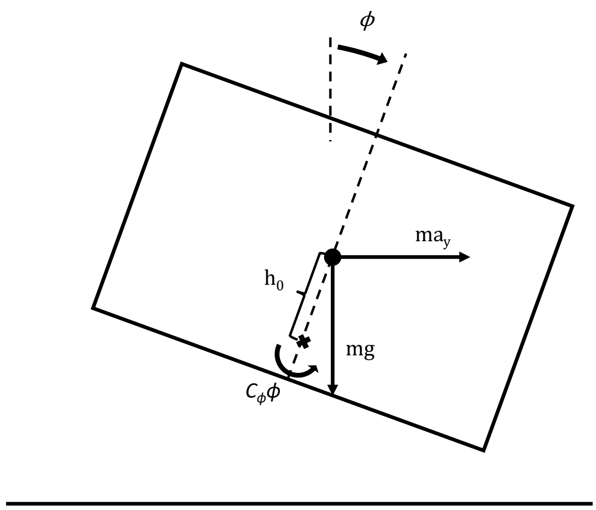

Figure 3.9: *Free body diagram of the vehicle rolling in steady state. The cross marks the roll center and the dot marks the center of gravity. $c_\phi\phi$ is the aligning moment from the springs.*

The roll axis is defined by two hard points which are determined by the suspension. Around each of these two points the front and the rear of the vehicle will roll respectively. The roll axis is the line which pass through both these points, and around which the entire car rolls. The lateral load transfer is calculated using moment equilibrium about the roll axis for either front or rear axle. Previously steady state was assumed, and if so, the sum of moments around the roll axis must equate to zero

$$(F_{z,i} - \Delta F_{z,i})w - (F_{z,i} + \Delta F_z)w - c_{\phi,i} - h_i F_{y,i} = 0 \tag{3.20}$$

where h_i is the i axle's roll height, ΔF_z is the lateral load transfer and w is the track width.

$$\Delta F_{z,i} = \frac{1}{2w}(\frac{c_{\phi,i}}{c_\phi - m_s h_0 g} + \frac{L-l_i}{L}h_i)m_s a_y = \frac{1}{2w}(c_{\phi,i}\phi + \frac{L-l_i}{L}m_s a_y) \tag{3.21}$$

The longitudinal load transfer is slightly different from the lateral. The load is assumed to divide evenly between left and right side of vehicle, which gives longitudinal load transfer according to

$$(\pm)\frac{m a_x h}{2L} \tag{3.22}$$

where a_x, is the longitudinal acceleration, h is the center of gravity height and L is the wheelbase of the vehicle. The longitudinal load transfer is positive for the rear axle. In the longitudinal direction the aerodynamic effects needs to be considered also. A point referred to as center of pressure is defined as the point where the drag and lift will act on the vehicle. The height of the center of pressure is referred to as h_p. The horizontal distance is referred to as l_p and is positive if center of gravity is in front of center of pressure. Assuming the aerodynamic forces always act in the longitudinal direction, the additional load due to aerodynamics is calculated as:

$$\frac{1}{4L}\rho A v^2 (C_l(L - l_i \pm l_p) \pm C_d h_p) \tag{3.23}$$

For front axle, subtraction is used where $\pm$ is specified, and for rear axle addition is used.

To conclude, the total load on a particular tire is equal to:

$$[h]F_{1z} = \underbrace{mg\frac{l_2}{2L}}_{\text{static load}} \underbrace{- \overbrace{\frac{1}{2w_1}(c_{\phi,1}\phi + \frac{L-l_1}{L}m_s a_y)}^{\text{lateral}} + \overbrace{\frac{m a_x h}{2L}}^{\text{longitudinal}}}_{\text{load transfer}} + \underbrace{\frac{1}{4L}\rho A v^2 (C_l(l_2 - l_p) - C_d h_p)}_{\text{aerodynamic effect}} \tag{3.24}$$

$$F_{2z} = mg\frac{l_2}{2L} + \frac{1}{2w_1}(c_{\phi,1}\phi + \frac{L-l_1}{L}m_s a_y) + \frac{m a_x h}{2L} + \frac{1}{4L}\rho A v^2 (C_l(l_2 - l_p) - C_d h_p) \tag{3.25}$$

$$F_{3z} = mg\frac{l_1}{2L} - \frac{1}{2w_2}(c_{\phi,2}\phi + \frac{L-l_2}{L}m_s a_y) - \frac{m a_x h}{2L}) + \frac{1}{4L}\rho A v^2 (C_l(l_1 + l_p) + C_d h_p) \tag{3.26}$$

$$F_{2z} = mg\frac{l_1}{2L} + \frac{1}{2w_2}(c_{\phi,2}\phi + \frac{L-l_2}{L}m_s a_y) - \frac{m a_x h}{2L} + \frac{1}{4L}\rho A v^2 (C_l(l_1 + l_p) + C_d h_p) \tag{3.27}$$

3.3.4 Motor model

The vehicle is propelled with two electric motors coupled to the rear wheels. These motors receive torque requests but the response will not be instantaneous. This is due to the fact that the motor torque requested by the vehicle control control is sent to the power electronic control module. This module contains a PID controller that converts the torque request into a current request. This current is then requested from the high voltage battery pack and supplied to the motors. Also the PID controller in the power electronic controller is tuned to be less responsive. This is done to prevent huge spikes in the current request that may cause over current situations.

In Figure 3.10 the measured torque from the motors along with the torque request is shown. The important feature to capture in the model is limitation on the torque rate, $\frac{dT}{dt}$. As shown in Figure 3.10 the output cannot shift to whatever reference is given. There is a lag between request and actual output. This behviour is modelled by simply saturating the output such that $|(T(t) - T(t + dt)| \leq \Delta T_{\max} dt$, where T is a discrete series of torque outputs, $\Delta T_{\max}$ is the highest allowed torque rate and dt is the sample time.

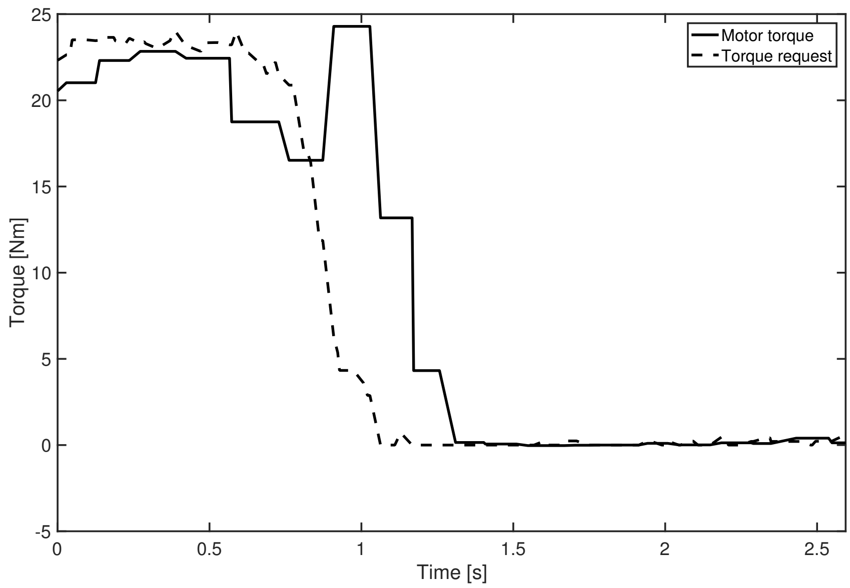

Figure 3.10: *Motor torque output and set value for motor controller. The data was collect from running one of the electric motors in a test cell.*

Besides being restricted by torque rate, the motors are limited by maximum torque output. At low speeds the motors tend to be limited by the maximum current that the coils can support. Since the output torque is proportional to the current, this leads to maximum torque being constant with respect to motor speed. At a certain speed the output power, torque multiplied by speed, will be higher than what the battery or power electronics can deliver. For engine speeds higher than this the propulsive torque will be limited power, and hence inversely proportional to motor speed. For safety reasons of the electric hardware a linear relation between torque and motor speed is used to limit the max torque of the motors.

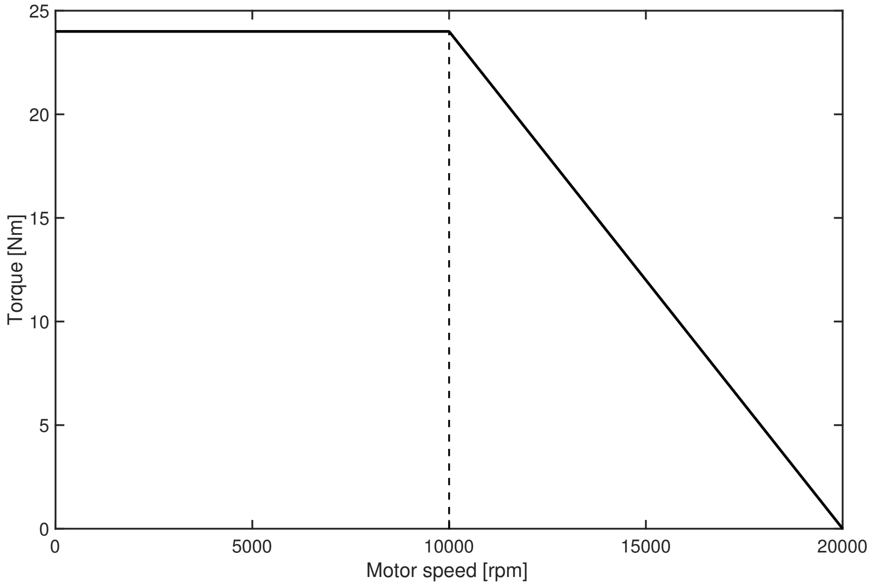

Figure 3.11: *Maximum torque output of one of the electric motors used.*

At very high speeds the motor is limited by the motor speed, and for such high speeds maximum torque is zero. Combing all these constrictions gives a maximum torque curve as shown in Figure 3.11. Numeric value for the different breakpoints have been taken from tests ran on the electric machines.

3.4 Vehicle control

As mentioned in the theory section, a model predictive control is used for yaw rate control. A simple block diagram of the MPC controller is shown in the Figure 3.12.

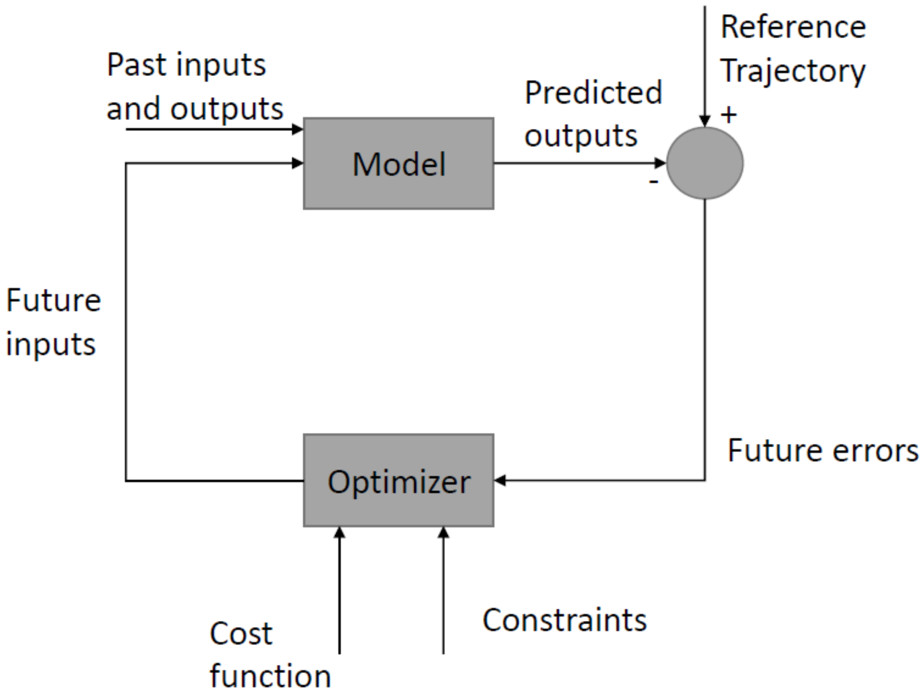

Figure 3.12: *Basic block diagram for an MPC controller.*

In an MPC Controller, a mathematical model (plant) of the system is used to calculate the future outputs. The outputs are then compared to the predicted future references to produce a future errors. A cost function is generated based on the errors and is optimised by an optimising algorithm. The optimiser gives optimised future inputs to the model which are used to calculate future outputs.

For the purpose of this thesis, the bicycle model was used as the plant for the controller. A state space formulation of the bicycle model was used for this purpose. A state space formulation is a combination of first order differential equations represented in the form of matrix equations. The system variables are called the states of the system. There are two types of state space formulations: Continuous time(CT) form and Discrete time(DT) form. The bicycle model is a continuous time model, but as the controller is to be used for the real time applications, a discrete time model is required. Hence, the CT form was converted to DT form.

3.4.1 Plant model

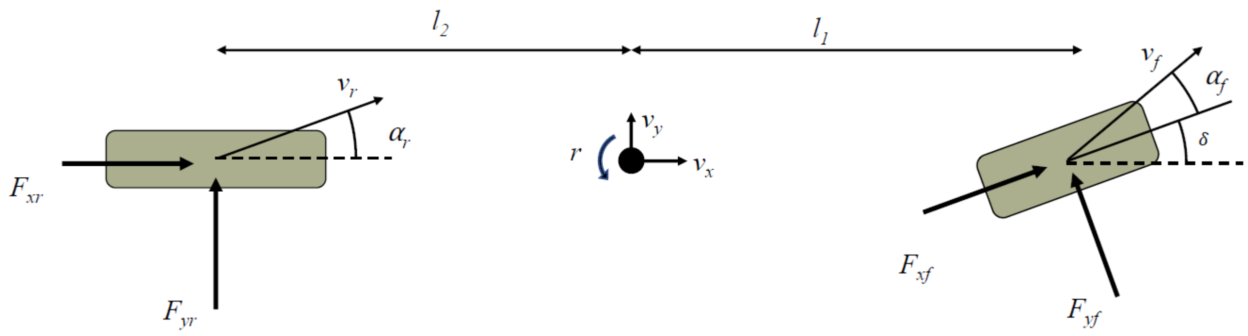

Figure 3.13: *Free body diagram of a one track model with front wheel steering.*

A free body diagram (FBD) for a one track model can be seen in figure 3.13. The model assumed that F_x is zero, hence v_x can be considered as constant. The force and moment equilibrium resulted into following equations

$$m(\dot{v}_y + v_x r) = F_{yf} + F_{yr} \tag{3.28}$$

$$I\dot{r} = l_1 F_{yf} + l_2 F_{yr} \tag{3.29}$$

The slip angles are assumed to be small. Thus, the lateral forces can be written as a linear function of the slip angle. The lateral force equation can be as follows

$$F_{yf} = C_f \alpha_f \tag{3.30}$$

$$F_{yf} = C_r \alpha_r \tag{3.31}$$

The slip angles are calculated by following equations

$$\alpha_f = \delta - \frac{1}{v_x}(v_y + l_1 r) \tag{3.32}$$

$$\alpha_r = -\frac{1}{v_x}(v_y - l_2 r) \tag{3.33}$$

From Eq. (3.28) to Eq. (3.33)

$$m\dot{v}_y + \frac{1}{v_x}(C_f + C_r)v_y + r\{mv_x + \frac{1}{v_x}(l_1 C_f - l_2 C_r)\} = C_f \delta \tag{3.34}$$

$$I_z\dot{r} + \frac{1}{v_x}(l_1^2C_f - l_2^2C_r)r + \frac{1}{v_x}(l_1C_f - l_2C_r)v_y = l_1C_f\delta \tag{3.35}$$

$$v_y = v_x\beta \tag{3.36}$$

Rearringing Eq. (3.34) and Eq. (3.35) and Eq. substituting (3.36)

$$\dot{\beta} + \{\frac{(C_1 + C_2)}{m}\}\beta + \{1 + \frac{l_1C_1 - l_2C_2}{mv_x^2}\}r = \{\frac{C_1}{mv_x}\}\delta \tag{3.37}$$

$$\dot{r} + \{\frac{(l_1C_1 - l_2C_2)}{I_z}\}\beta + \{\frac{(l_1^2C_1 - l_2^2C_2)}{I_z}\}r = \{\frac{l_1C_1}{I_z}\}\delta \tag{3.38}$$

In order to include torque vectoring in the model, an external yaw moment (M_z) is added to the Eq. (3.38). This moment is translated into the yaw acceleration ($\dot{r}$) by dividing it with yaw inertia (I_z). Thus the Eq. (3.38) can be re-written as

$$\dot{r} + \{\frac{(l_1C_1 - l - 2C_2)}{I_z}\}\beta + \{\frac{(l_1^2C_1 - l_2^2C_2)}{I_z}\}r = \{\frac{l_1C_1}{I_z}\}\delta + \{\frac{1}{I_z}\}M_z \tag{3.39}$$

Thus using matrix equation form for Eq. (3.37) and (3.39),

$$\begin{bmatrix}\dot{\beta} \\ \dot{r}\end{bmatrix} = \begin{bmatrix} -\frac{(C_1+C_2)}{m} & -(1 + \frac{l_1C_1 - l_2C_2}{mv_x^2}) \\ -\frac{(l_1C_1 - l_2C_2)}{I_z} & -\frac{(l_1^2C_1 - l_2^2C_2)}{I_z}\end{bmatrix}\begin{bmatrix}\beta \\ r\end{bmatrix} + \begin{bmatrix}\frac{C_1}{mv_x} & 0 \\ \frac{l_1C_1}{I_z} & \frac{1}{I_z}\end{bmatrix}\begin{bmatrix}\delta \\ M_z\end{bmatrix} \tag{3.40}$$

From Eq. (3.40), β and r are the states of the system and δ and M_z are the inputs to the system. Comparing it with the standard state space form for continuous time $\dot{x} = Ax + Bu$,

$$x = \begin{bmatrix}\beta \\ r\end{bmatrix}, A = \begin{bmatrix} -\frac{(C_1+C_2)}{m} & -(1 + \frac{l_1C_1 - l_2C_2}{mv_x^2}) \\ -\frac{(l_1C_1 - l_2C_2)}{I_z} & -\frac{(l_1^2C_1 - l_2^2C_2)}{I}\end{bmatrix}, B = \begin{bmatrix}\frac{C_1}{mv_x} & 0 \\ \frac{l_1C_1}{I_z} & \frac{1}{I_z}\end{bmatrix}, u = \begin{bmatrix}\delta \\ M_z\end{bmatrix} \tag{3.41}$$

Here, M_z can not be used directly as an input to the physical system i.e. the vehicle. Hence, M_z needs to be converted to motor torque which is a valid input to the vehicle. The relation between M_z and motor torque can be given as

$$M_z = \{\frac{G_{\text{ratio}}w_2}{R_w}\}\Delta T_m \tag{3.42}$$

Hence, for a positive M_z the torque on left and right wheels can be written as

$$Tm_{\text{left}} = Tm - \Delta Tm \tag{3.43}$$
$$Tm_{\text{right}} = Tm + \Delta Tm \tag{3.44}$$

The output of the system can be given by

$$y = Cx \tag{3.45}$$

Matrix C can be selected depending on the output required from the system.

The continuous time model shown in Eq. (3.40) is converted into discrete time model by performing various modifications. It is assumed that the for a given time step (ts) $\dot{x}$ is constant and thus it can be represented as function of discrete time (t)

$$\dot{x} = \frac{x(t+1) - x(t)}{ts} \tag{3.46}$$

Thus the continuous time state space form can be written as

$$\frac{x(t+1) - x(t)}{ts} = Ax(t) + Bu(t) \tag{3.47}$$

$$x(t+1) = \{(I + A)ts\}x(t) + \{Bts\}u(t) \tag{3.48}$$

From Eq. (3.48) $A_d = (I + A)ts$ and $B_d = Bts$, where A_d and B_d are discrete time matrices, thus the discrete time equation can be written as

$$x(t+1) = A_d x(t) + B_d u(t) \tag{3.49}$$

Eq. (3.49) is used as plant model for the MPC controller.

3.4.2 Controller design

In the first step, the model is converted to the incremental state model. In this model the input u(t) is replaced with $\Delta u(t)$, where $\Delta u(t) = u(t) - u(t-1)$ and a new state u(t-1) is introduced. Thus the new state space model can be given as

$$\begin{bmatrix} x(t+1) \\ u(t) \end{bmatrix} = \begin{bmatrix} A & B \\ 0 & I \end{bmatrix} \begin{bmatrix} x(t) \\ u(t-1) \end{bmatrix} + \begin{bmatrix} B \\ I \end{bmatrix} \begin{bmatrix} \Delta u(t) \end{bmatrix} \tag{3.50}$$

$$y(t) = \begin{bmatrix} C \\ 0 \end{bmatrix} \begin{bmatrix} x(t) \\ u(t-1) \end{bmatrix} \tag{3.51}$$

Eq. (3.50) and Eq. (3.51) can be written with new notations as

$$X(t+1) = MX(t) + NU(t) \tag{3.52}$$

$$y(t) = QX(t) \tag{3.53}$$

where,

$$X = \begin{bmatrix} x(t) \\ u(t-1) \end{bmatrix}, M = \begin{bmatrix} A & B \\ 0 & I \end{bmatrix}, N = \begin{bmatrix} B \\ I \end{bmatrix}, Q = \begin{bmatrix} C & 0 \end{bmatrix}, U = \begin{bmatrix} \Delta u(t) \end{bmatrix} \tag{3.54}$$

In order to access the future states a regression of Eq. (3.50) is used,

$$\begin{aligned} y(t+1) &= QMX(t) + QNU(t) \\ y(t+2) &= QM^2X(t) + QMNU(t) + QNU(t+1) \\ &. \\ &. \\ &. \\ y(t+j) &= QM^jX(t) + \sum_{i=0}^{j-1} QM^{j-i-1}NU(t+i) \end{aligned}$$

This system of equations can be represented in simple form as

$$y_{\text{reg}} = FX_{\text{reg}} + HU_{\text{reg}} \tag{3.55}$$

where,

$$F = \begin{bmatrix} QM \\ QM^2 \\ . \\ . \\ QM^{Nh} \end{bmatrix}, H = \begin{bmatrix} QN & 0 & ... & 0 \\ QMN & QN & ... & 0 \\ . & . & . & . \\ . & . & . & . \\ QM^{Nh-1}N & .... & QMN & QN \end{bmatrix}, \tag{3.56}$$

In Eq. (3.56) Nh is called the prediction horizon. This quantity determines the number of steps for which future states are determined. In order to obtain an optimised input, a cost function is selected based on the error to the reference and input. The reference matrix is the predicted reference at each time step up to Nh. Thus. $\text{ref} = [\text{ref}(t+1), \text{ref}(t+2), ..., \text{ref}(t+Nh)]^T$. The cost function is written as

$$J = (y_{\text{reg}} - \text{ref})^T R_w (y_{\text{reg}} - \text{ref}) + U_{\text{reg}}^T Q_w U_{\text{reg}}$$

$$J = (FX_{\text{reg}} + HU_{\text{reg}} - \text{ref})^T R_w (FX_{\text{reg}} + HU_{\text{reg}} - \text{ref}) + U_{\text{reg}}^T Q_w U_{\text{reg}} \tag{3.57}$$

Here, R_w and Q_w are weight matrices. $R_w = \text{diag}(r_w, r_w ... r_w)$ and $Q_w = \text{diag}(q_w, q_w ... q_w)$.

In reality, most of the systems operates within finite constraints. These constraints might be due to limitations imposed by mechanics, electronics, system safety etc. The system might get unstable if these limitations are exceeded. To remedy this, there are algorithms that perform constrained optimisation. One such algorithm known as quadratic optimisation was used to calculate the optimum inputs.

3.4.3 Quadratic optimisation

The base equation for quadratic optimisation is required in the form of Eq. (3.58)

$$J = x^T H_q x + b_q x + f_0 \tag{3.58}$$

where H_q is a positive semi-definite symmetric matrix. b_q and f_0 are constant matrices. The cost function formulated in Eq. (3.57) can be written into the quadratic form. The constrains for the given system are the mechanical limitation on the steering and motor torque. But as the U_{reg} is a matrix consisting of Δu, the constraints are written as,

$$lU_{\max} < TU_{\text{reg}} + u(t-1) < lU_{\min} \tag{3.59}$$

Here l is a (Nh $\times$ m) $\times$ n size matrix formed of Nh $m \times n$ identity matrices, given that the system has m inputs and n outputs. T is a lower triangular block matrix, with the blocks made of identity matrices. $U_{\max}$ and $U_{\min}$ are the upper and lower constraints for the input.

For example, if m = 2, n = 2 and Nh = 3

$$l = \begin{bmatrix} 1 & 0 \\ 0 & 1 \\ 1 & 0 \\ 0 & 1 \\ 1 & 0 \\ 0 & 1 \end{bmatrix}, T = \begin{bmatrix} 1 & 0 & 0 & 0 & 0 & 0 \\ 0 & 1 & 0 & 0 & 0 & 0 \\ 1 & 0 & 1 & 0 & 0 & 0 \\ 0 & 1 & 0 & 1 & 0 & 0 \\ 1 & 0 & 1 & 0 & 1 & 0 \\ 0 & 1 & 0 & 1 & 0 & 1 \end{bmatrix}, U_{\max} \begin{bmatrix} u_{\max1} \\ u_{\max2} \\ u_{\max1} \\ u_{\max2} \\ u_{\max1} \\ u_{\max2} \end{bmatrix}, U_{\min} = \begin{bmatrix} u_{\min1} \\ u_{\min2} \\ u_{\min1} \\ u_{\min2} \\ u_{\min1} \\ u_{\min2} \end{bmatrix}$$

Thus, using the incremental form ($\Delta u(t)$) makes the computation process more complicated. In order to reduce the computation complication, the incremental form can be converted to the normal form (u(t)) as follows.

$$U_{\text{reg}} = \begin{bmatrix} u(t) - u(t-1) \\ u(t+1) - u(t) \\ u(t+2) - u(t+1) \\ . \\ . \\ u(Nh) - u(Nh-1) \end{bmatrix} = \begin{bmatrix} 1 & 0 & 0 & \dots & 0 \\ -1 & 1 & 0 & \dots & 0 \\ 0 & -1 & 1 & \dots & 0 \\ . & . & . & \dots & . \\ . & . & . & \dots & . \\ 0 & 0 & 0 & \dots & 1 \end{bmatrix} \begin{bmatrix} u(t) \\ u(t+1) \\ u(t+2) \\ . \\ . \\ u(Nh) \end{bmatrix} - \begin{bmatrix} u(t-1) \\ 0 \\ 0 \\ . \\ . \\ 0 \end{bmatrix} \tag{3.60}$$

The above Eq. (3.60) can be written as

$$U_{\text{reg}} = DU_s - f_1 \tag{3.61}$$

Substituting Eq. (3.61) in Eq. (3.57)

$$J = (FX_{\text{reg}} + H(DU_s - f_1) - \text{ref})^T R_w (FX_{\text{reg}} + H(DU_s - f_1) - \text{ref}) + (DU_s - f_1)^T Q_w (DU_s - f_1) \tag{3.62}$$

Taking f_2 and G as,

$$f_2 = FX_{\text{reg}} - Hf_1 \tag{3.63}$$
$$G = HD \tag{3.64}$$

On simplification of Eq. (3.62),

$$\begin{aligned} J = U_s^T (G^T R_w G + D^T Q_w D) U_s + 2[(f_2 - \text{ref})^T R_w G^T - f_1^T Q_w D] U_s^T + \\ ((f_2 - \text{ref}))^T R_w ((f_2 - \text{ref})) + f_1^T Q_w f_1 \end{aligned} \tag{3.65}$$

Comparing with Eq. (3.58),

$$
\begin{aligned}
H_q &= 2(G^T R_w G + D^T Q_w D) \\
b_q &= 2[(f_2 - \text{ref})^T R_w G^T - f_1^T Q_w D] \\
f_0 &= ((f_2 - \text{ref}))^T R_w ((f_2 - \text{ref})) + f_1^T Q_w f_1
\end{aligned}
$$

and the constraints can be written as

$$U_{\max} < U_s < U_{\min}$$

Then using H_q, b_q and f_0 as inputs to the quadratic optimisation, the optimum inputs (u*) can be obtained.

3.4.4 State observer

In the controller design, the bicycle model is used as a plant. Due to its simplicity, the model can not estimate the actual states of the vehicle. The actual vehicle states are measurable due to the sensors present on the vehicle. Hence, the states estimated by the model and the measured state can be used together to generate a better estimation of the state. This estimation method is called a state observer. The state ($\hat{x}$) can be estimated by

$$\hat{x}(t) = A\hat{x}(t-1) + Bu(t-1) + L(y(t) - \hat{y}) \tag{3.66}$$

where, $\hat{y}$ is the measured output of the system and L is called the observer gain matrix. The eigen value method was chosen to calculate the value of L. In this method, stable eigen values are selected for A-LC and value of L is calculated. Sylvester equation was used to calculate the value of L. The Sylvester equation is given as

$$A^T X - X\Lambda = C^T G \tag{3.67}$$

$$L^T = GX^{-1} \tag{3.68}$$

Here Λ is a diagonal matrix with desired eigen values ($\text{diag}(\lambda_1, \lambda_2, ...\lambda_n)$). The matrix G is an arbitrary matrix.

(3.67) is used to compute the matrix X. As the matrix M^T is a $n \times n$ matrix, X was also assumed to be a $n \times n$ matrix.

$$X = \begin{bmatrix} x_{11} & x_{12} & x_{13} & ... & x_{1n} \\ x_{21} & x_{22} & x_{23} & ... & x_{2n} \\ . & . & . & ... & . \\ . & . & . & ... & . \\ x_{n1} & x_{n2} & x_{n3} & ... & x_{nn} \\ \end{bmatrix} \tag{3.69}$$

Eq. (3.69) in Eq. (3.67), a system of n equations with n variables is obtained. Assuming, $x = [x_{11}, x_{12}, ...x_{nn}]^T$, a coefficient matrix (C) and a solution matrix (S) can be obtained. Then, the matrix x can be computed as,

$$x = C^{-1}S \tag{3.70}$$

Eq. (3.70) was used to get the matrix X which was then used to compute L by using Eq. (3.68).

3.4.5 Controller versions

As specified in the research question posed by this thesis, a comparison of two control system is required. One of these control system uses the side-slip angle control while the other system does not. Therefore, two versions of the MPC controller were created.

Controller without side slip control

In this case, the system output (y) is only the yaw rate (r). Hence, the output equation is written as

$$y = \begin{bmatrix} 0 & 1 \end{bmatrix} \begin{bmatrix} \beta \\ r \end{bmatrix} \tag{3.71}$$

Therefore,

$$C = \begin{bmatrix} 0 & 1 \end{bmatrix}, Q = \begin{bmatrix} 0 & 1 & 0 \end{bmatrix} \tag{3.72}$$

Furthermore, in Eq. (3.66), $\hat{y}$ is the measured value of the yaw rate from the vehicle's interial measurement unit (IMU).

$$y = r_{\text{measd}} \tag{3.73}$$

The reference matrix used in Eq. (3.62) consists of future yaw rate reference predicted in the Lateral reference section. If Nh is the prediction horizon then,

$$\text{ref} = \begin{bmatrix} yaw_{\text{ref}}(t+1) \\ yaw_{\text{ref}}(t+2) \\ . \\ . \\ yaw_{\text{ref}}(t+Nh) \end{bmatrix} \tag{3.74}$$

Also the controller parameters, R_w and Q_w used in Eq. (3.62) were tuned using a sine wave track. The 3.15 and 3.14 shows the controller behaviour for two different values for R_w and Q_w.

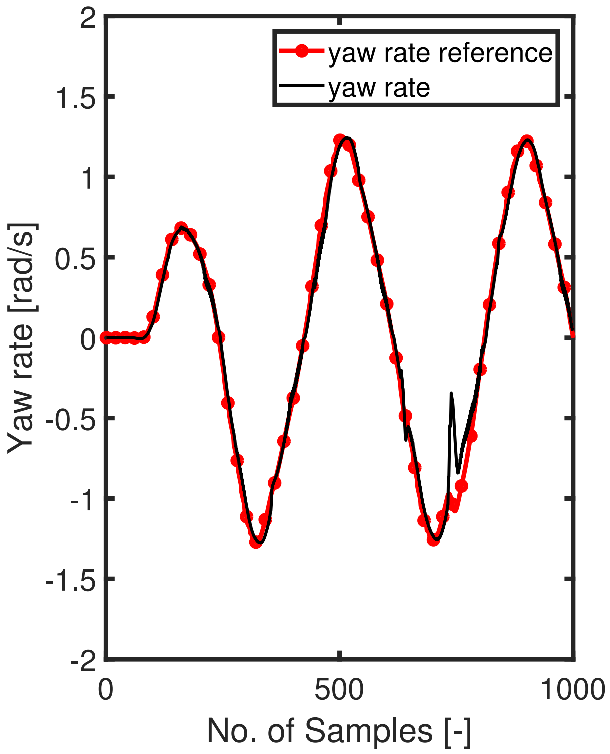

Figure 3.14: *Yaw rate vs reference yaw rate for a sine wave track ($q = 2$, $r_w = 100$).*

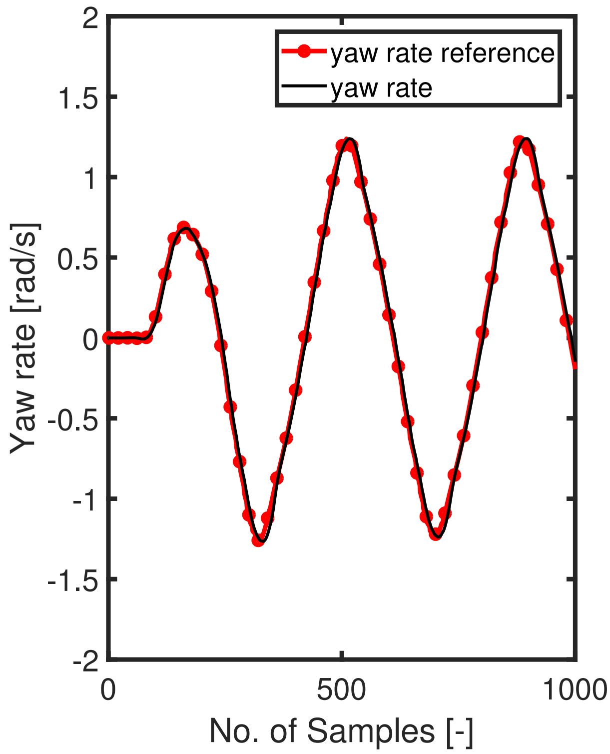

Figure 3.15: *Yaw rate vs reference yaw rate for a sine wave track ($q = 40$, $r_w = 10$).*

Controller with side slip control

In this case, the system output (y) is the yaw rate (r) and side slip (β). Hence, the output equation is written as

$$y = \begin{bmatrix} 1 & 0 \\ 0 & 1 \end{bmatrix} \begin{bmatrix} \beta \\ r \end{bmatrix} \tag{3.75}$$

Therefore,

$$C = \begin{bmatrix} 1 & 0 \\ 0 & 1 \end{bmatrix}, \quad Q = \begin{bmatrix} 1 & 0 & 0 \\ 0 & 1 & 0 \end{bmatrix} \tag{3.76}$$

Furthermore, in Eq. (3.66), $\hat{y}$ is a matrix with measured value of side slip angle via the side slip estimator and the yaw rate from the vehicle's interial measurement unit (IMU).

$$y = \begin{bmatrix} \beta_{\text{meas}} \\ r_{\text{meas}} \end{bmatrix} \tag{3.77}$$

The reference matrix used in Eq. (3.62) will contain future yaw rate reference as well as future side slip reference. The side slip reference is selected to be zero, because when $\beta = 0$, lateral shift from the path is minimum. If Nh is the prediction horizon then,

$$\text{ref} = \begin{bmatrix} 0 \\ yaw_{\text{ref}}(t+1) \\ 0 \\ yaw_{\text{ref}}(t+2) \\ . \\ . \\ 0 \\ yaw_{\text{ref}}(t+Nh) \end{bmatrix} \tag{3.78}$$

The controller parameters, R_w and Q_w used in Eq. (3.62) were tuned using a sine wave track. Figure 3.17 and 3.16 shows the controller behaviour for two different values for R_w and Q_w. It can be seen from the Figure 3.14 that a poor choice of the parameters leads to erratic controller behaviour.

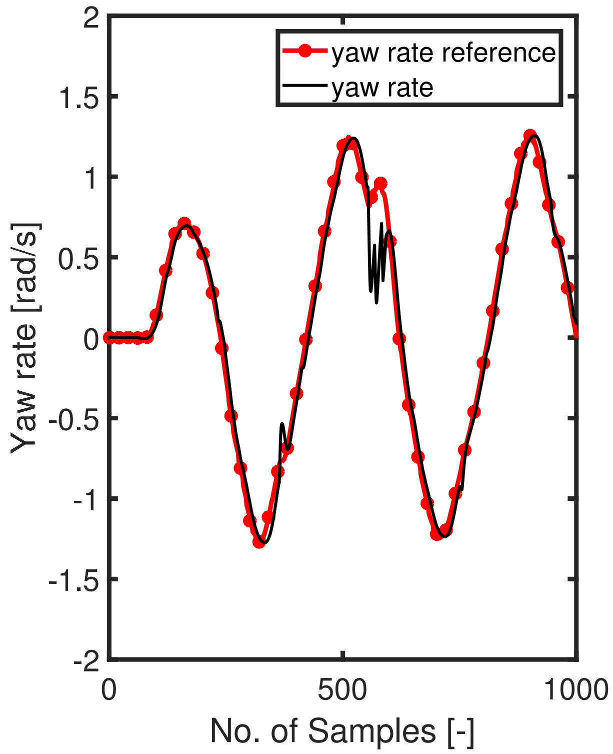

Figure 3.16: *Yaw rate vs reference yaw rate for a sine wave track* ($q_w = 120$, $r_w = 1$).

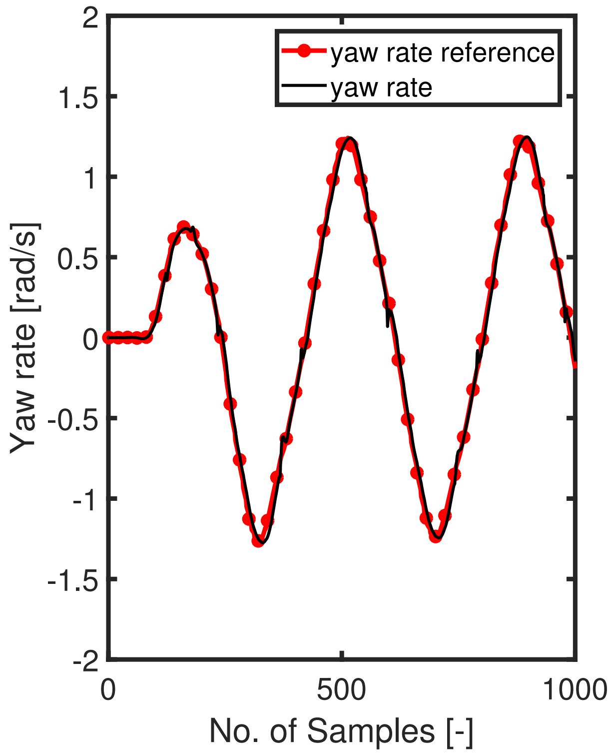

Figure 3.17: *Yaw rate vs reference yaw rate for a sine wave track* ($q_w = 45$, $r_w = 20$).

3.5 Side slip estimation

Side slip is the angular difference between a vehicles velocity and the longitudinal direction. To estimate this angle, this thesis utilised the perception sensors equipped on new generation vehicles. With the help of camera and LIDAR a 2D-map is built of the vehicle's surrounding. Changes in the map are tracked over time, and static objects are identified. By differentiating the relative position between the vehicle and the static objects with respect to time, it is possible to estimate the vehicle's velocity.

Each cluster of points detected by the perception is stored as a position in the vectors X_t and Y_t. The positions are compared with the clusters found in the previous time step, X_{t-1} and Y_{t-1}. The distance a point can move between frames is estimated to

$$\frac{1}{f}\left(v + \frac{a}{2f} + r\sqrt{X_{t-1}^2 + Y_{t-1}^2}\right)$$

where v is the vehicle's velocity, a its acceleration, r its yaw rate and f the frequency of the perceptive unit. Which can be used to filter which points are reoccurring in consecutive frames.

Because the vehicle is, or at least might, be rotating, the positions (X_t, Y_t) and $(X_t - 1, Y_{t-1})$ are not in the same coordinate system. To transfer them to the same coordinate system, the rotation of the vehicle is needed and can be accessed from the inertial measurement unit (IMU). Assuming the vehicle has turned an angle of θ at a constant rate, the positions of (X_t, Y_t) can be expressed in $(X_t - 1, Y_{t-1})$ coordinate frame according to

$$\begin{bmatrix} X_t^{t-1} \\ Y_t^{t-1} \end{bmatrix} = \begin{bmatrix} cos(\theta) & sin(\theta) \\ -sin(\theta) & cos(\theta) \end{bmatrix} \begin{bmatrix} X_t \\ Y_t \end{bmatrix}$$

How much the vehicle has moved between the frames can be approximated to

$$\begin{bmatrix} X_t^{t-1} - X_{t-1} \\ Y_t^{t-1} - Y_{t-1} \end{bmatrix}$$

which when differentiated gives an estimation of the velocity in x and y direction.

Every static object found in the vehicle's surrounding gives an approximation of the velocity. Outliers are filtered out with respect to acceleration limits of the vehicle. Of the remaining, an average velocity is calculated and used as an estimate. Since the relative orientation between the camera, LIDAR and vehicle is known, the difference between the direction of the velocity and heading is also known.

3.6 Validation

To evaluate the control system, four test scenarios have been used. The evaluation criteria are stated in the problem statement (see 1.1).

FSG track On the full FSG track, shown in Figure 3.18, the lap time and average yaw rate deviation are measured.

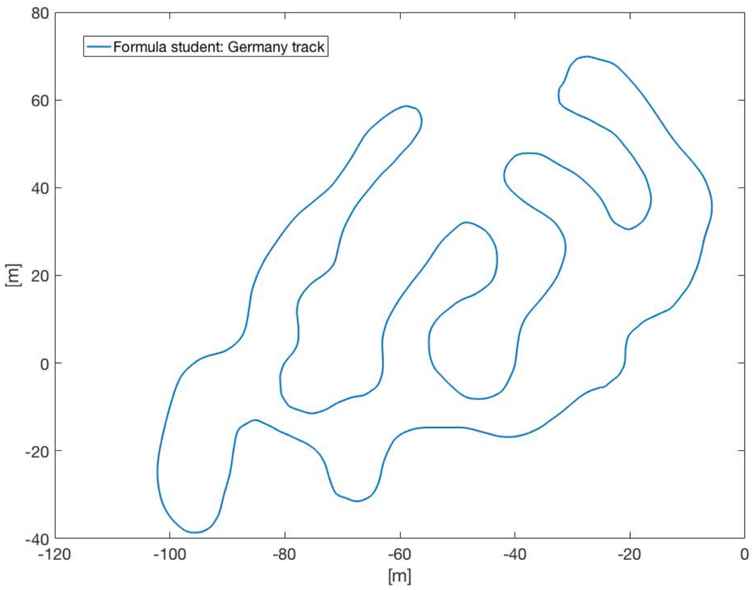

Figure 3.18: *Formula Student Germany track layout.*

Double lane change In the double lane change scenario, the controller's response properties rise time and overshoot was measured.

Sine wave with dwell In the sine wave with dwell scenario, the controller's response properties rise time and overshoot was measured. This test is an efficient way to instigate over-steer situations according to [21].

Step response Zero steering reference is given until a sudden step. This method is accurate when measuring the response of a system, and can easily determine rise time and overshoot.

4 Result

This section covers the results of the thesis. The first subsection includes the results from the simulation. Four different driving scenarios were tested in simulation, a track drive, step response, sine wave with dwell and a double lane change manoeuvre. These test cases capture the difference between yaw control with and without as an input side slip. The yaw controller's performance is based on track deviation, rise time, overshoot and lap time. The track drive is mainly be used to measure the lap time, average track deviation, as well as give a broad view of how well the yaw reference is kept. The rise time is measured from the step response, and overshoots from step response, sine wave and double lane change.

4.1 Simulation results

The results of the simulations are covered in the following subsection. A two track model was used to simulate a step response, double lane change, sine with dwell and driving on the FSG track. Results are shown for two different concepts, referred to as the *yaw–beta controller* and the *yaw controller*, with the difference being the yaw–beta controller trying to minimise body side slip of the vehicle. Both are explained more in depth in Section 3.4.

4.1.1 Step response

The step response is simulated by increasing the yaw reference by a step. The step was performed at close to 50 km/h. The yaw rate measured by the yaw–beta controller is shown in Figure 4.1 and the rise time, defined as the time taken to achieve 90% of the reference step, is equal to 70.8 ms. The yaw–beta controller had no overshoot.

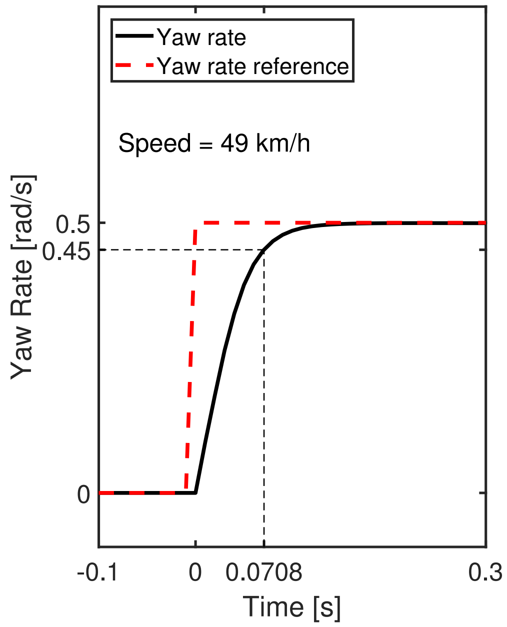

Figure 4.1: *Step response to a yaw reference with the use of a slip estimator*

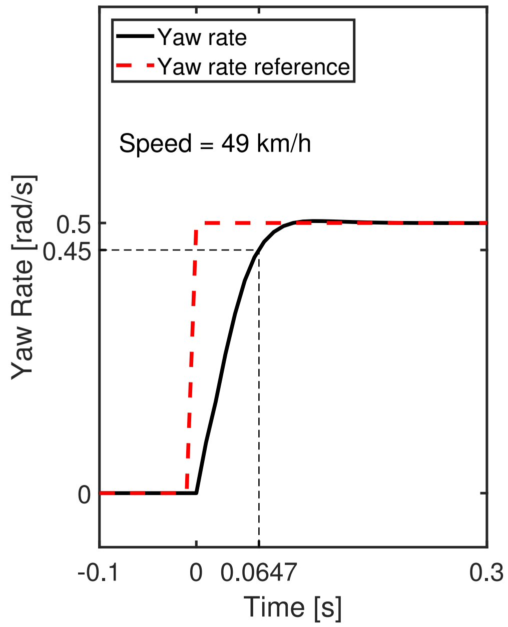

Figure 4.2: *Step response to a yaw reference without the use of a slip estimator*

In Figure 4.2 the results from the yaw controller is presented. The yaw controller's rise time is equal to 64.7 ms and the overshoot of the yaw controller is 0.0036 rad/s.

In Figure 4.3 the side slip angles for both test cases are shown. The peak side slip angle of the yaw controller, 0.77°, is 4.13% higher than the peak side slip of the yaw–beta controller, 0.64°.

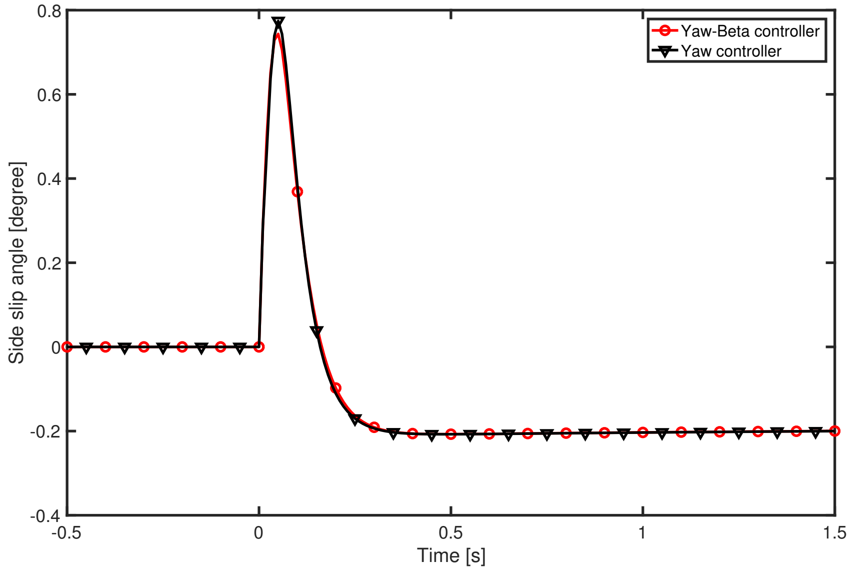

Figure 4.3: *Side slip angle for a step response with the yaw–beta controller and the yaw controller.*

4.1.2 Double lane change

The double lane change captures the dynamics of an overtake. In Figure 4.4 the trajectory of the double lane change is shown, for both versions of the controller. The figures shows both vehicles passing the test, by driving through all the gates.

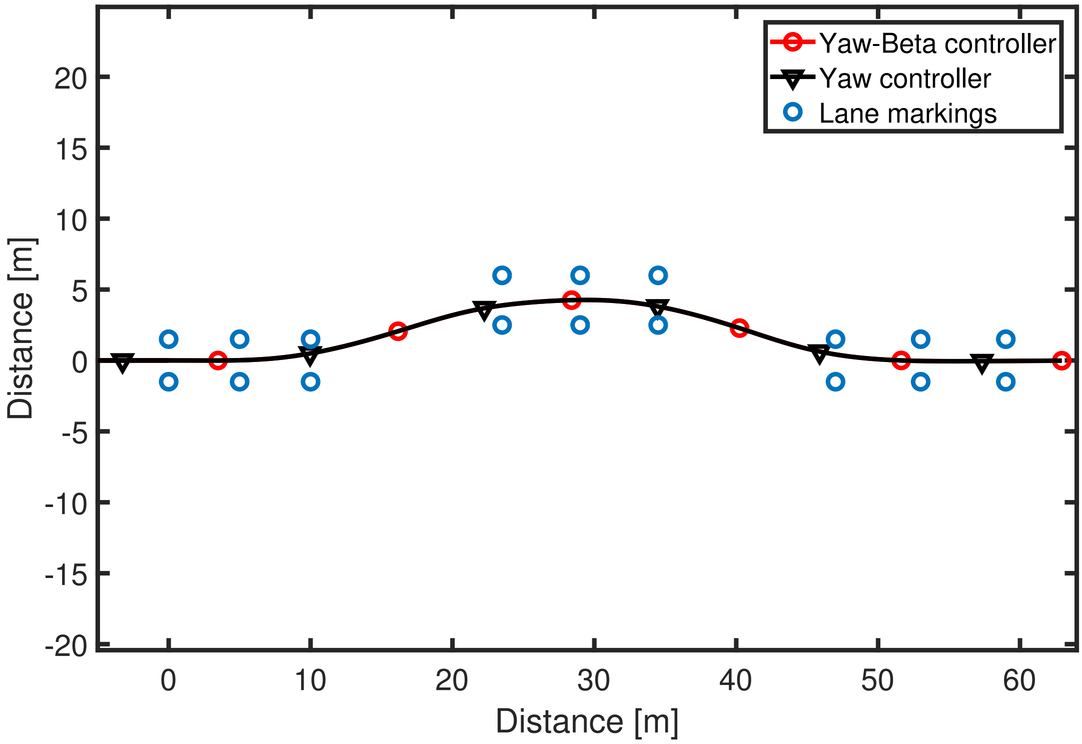

Figure 4.4: *The trajectory covered for two double lane change manoeuvres with different control systems. The red curve marked with is the yaw–beta controller, while the black curve marked with triangles is the the yaw controller. The blue markers represent cones which the vehicle must pass through*

In Figure 4.5 the side slip angle for both controllers during the double lane change manoeuvre is shown. The yaw–beta and the yaw controller achieved similar side slip angles throughout the manoeuvre.

4.1.3 Sine wave with dwell

The reference to the controllers is given as a sine wave, with a dwell on the latter peak. In Figure 4.6 the yaw rate reference and the measured yaw rate are displayed for the yaw–beta controller. In Figure 4.7 the yaw rate reference and the measured yaw rate are shown for the yaw controller. The test was carried out at approximately 50 km/h.

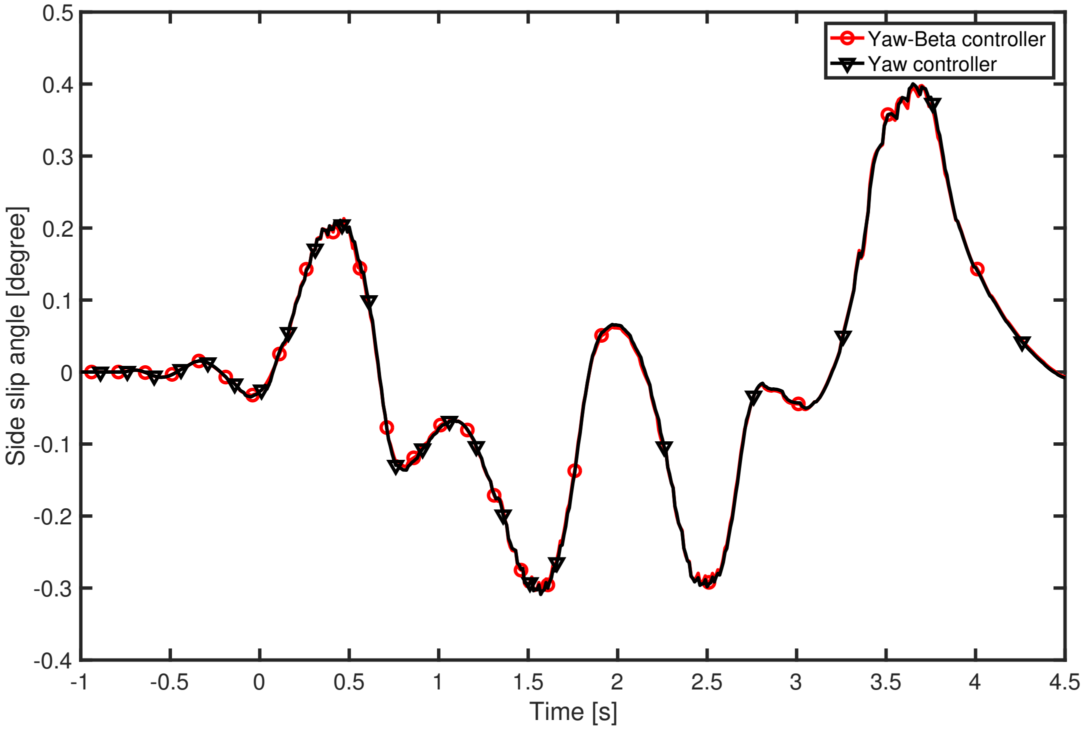

Figure 4.5: *Body side slip angle from a double lane change manoeuvre. The red curve marked with circles is the yaw–beta controller, while the black curve marked with triangles is the yaw controller.*

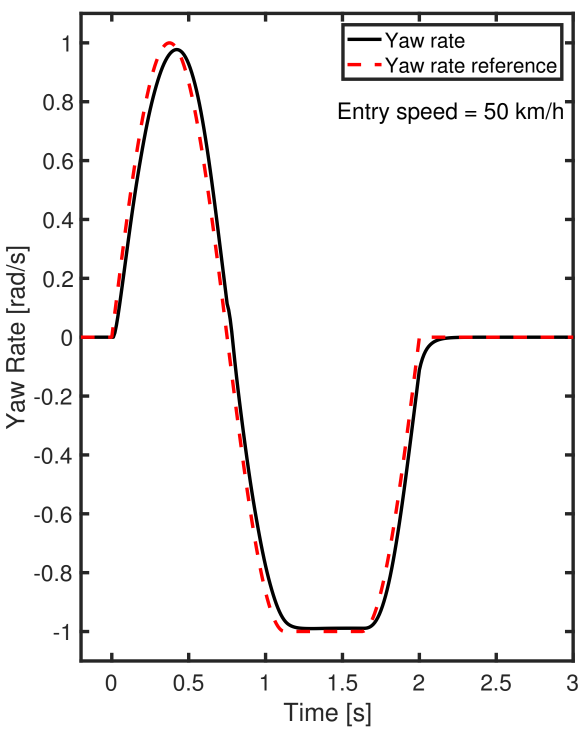

Figure 4.6: *A sine wave yaw rate reference with a dwell at the last peak. This was performed with yaw–beta control.*

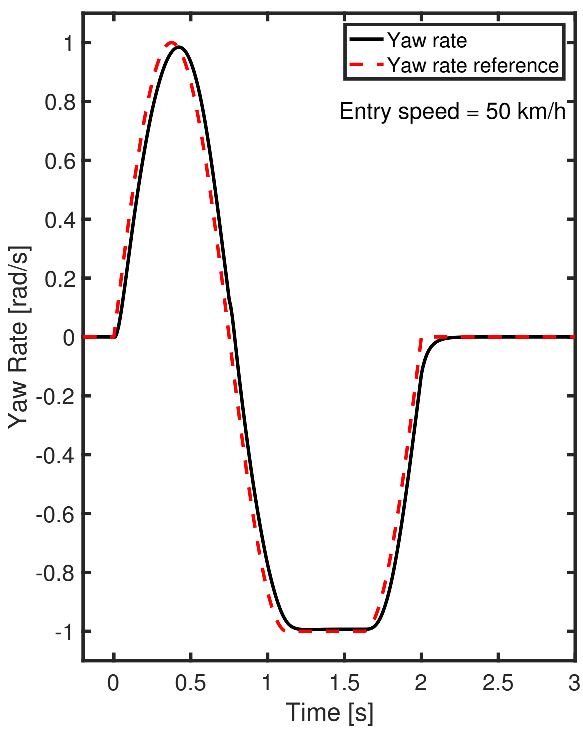

Figure 4.7: *A sine wave yaw rate reference with a dwell at the last peak. This was performed with yaw control.*

The time taken to reach -0.1 rad/s yaw rate after the sine dwell for the yaw–beta controller was 375.3 ms, whereas the yaw controller need 380.9 ms for the same yaw rate change. Neither of the two systems produced any overshoot of significance.

In Figure 4.8 the side slip angle for both controllers during the sine dwell manoeuvre is presented. Both control systems achieved similar side slip angles.

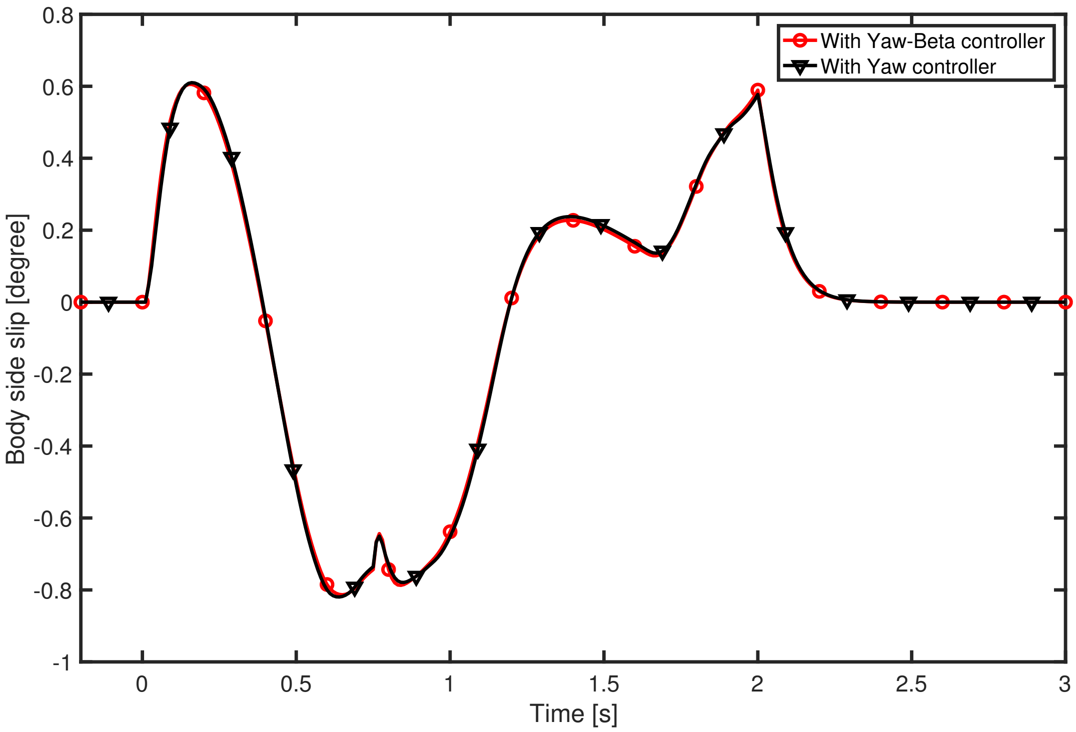

Figure 4.8: *Body side slip during sine with dwell manoeuvre of both the yaw–beta and the yaw controller.*

4.1.4 Track drive

The track drive is simulated for one lap, for each of the control systems. The map layout used is an endurance track from the Formula Student Germany (FSG) competition.

Disparity maps between the yaw–beta controller and the yaw controller are plotted for some important parameters for a lap on the FSG map. As different controllers are used while simulating the lap, the time taken by the vehicle in each scenario is different. Thus, a direct comparison of two data sets is not possible. To overcome this problem, both the data sets are are equalised by diving one data set into same number of data points as the other. This division is based on the ratio of the distance of each point from the start point to the total distance of the track. Then, the parameters of interest are interpolated to get a one to one coincidence with the data from other data set.

As a quality control of the controller comparison a longitudinal velocity disparity and lateral deviation disparity map are used. side slip angle disparity between the yaw–beta controller and the yaw controller for the vehicle are scattered on the map to assess the performance of the two concepts.

From Figure 4.9, it is seen that the velocity disparity scatter is quite close to zero. As all the comparison parameters are velocity dependent, this zero velocity disparity makes the parameter comparison more robust and valid. If the velocity disparity of the two vehicles becomes large relative to the absolute velocity, comparing lateral displacement and body side slip would be inconsequential. The maximum velocity difference is 2.82 m/s.

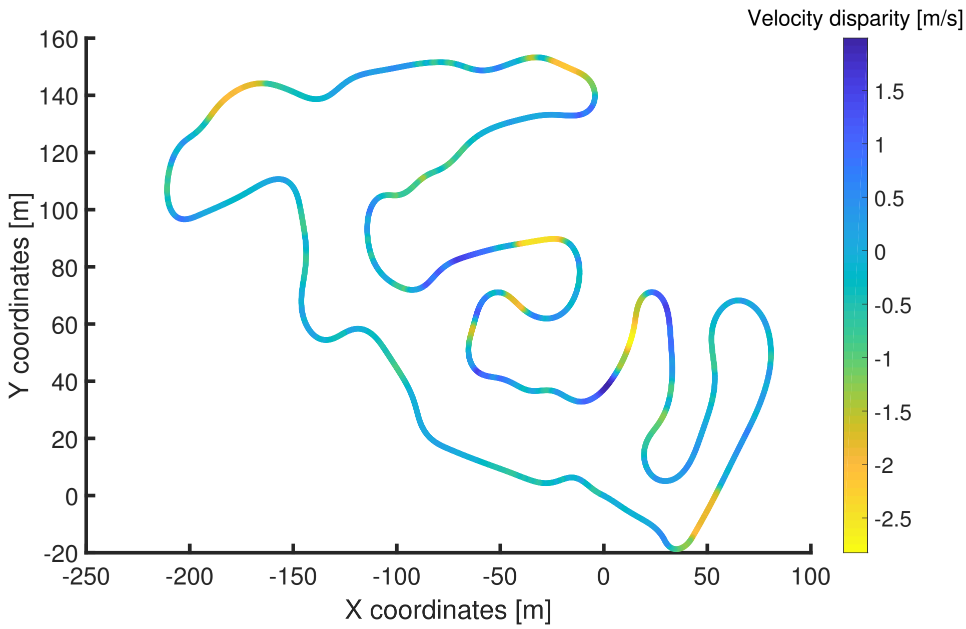

Figure 4.9: *Velocity disparity between the yaw–beta controller and the yaw controller.*

It can be seen from Figure 4.10, the highest lateral deviation disparity is 0.992 m. Its should also be mentioned that the absolute values of the lateral deviation are quite small (less than 1 m), hence the vehicle adheres the track quite admirably while sustaining respectable speeds.

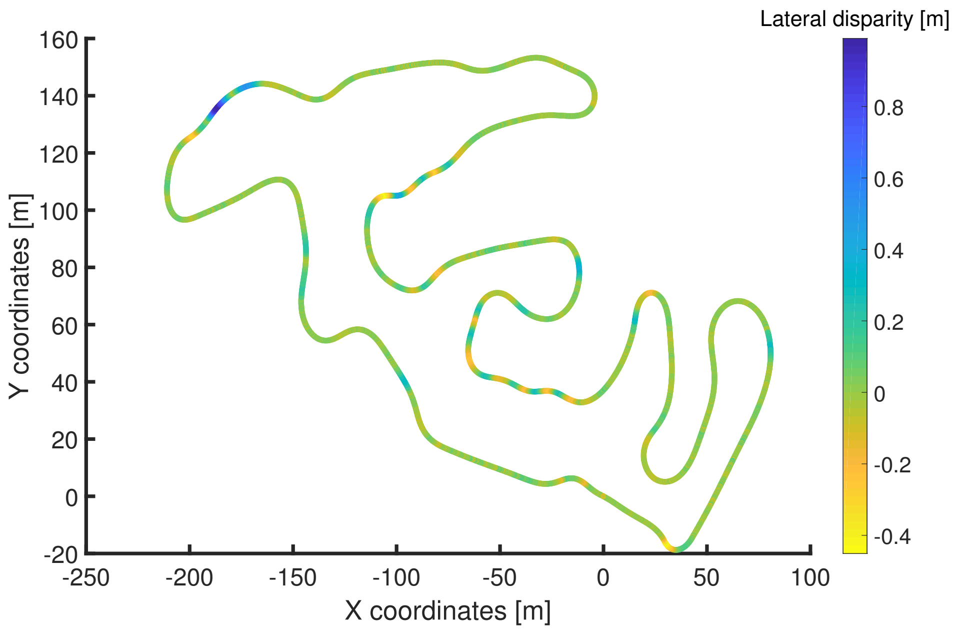

Figure 4.10: *Lateral deviation disparity between the yaw–beta controller and yaw controller.*

Side slip angle disparity is shown in Figure 4.11. It can be seen that the disparity values are as high as 12.46 deg. The higher values of disparity occurs at specific parts of the track only but for the majority of the track the disparity is quite close to zero.

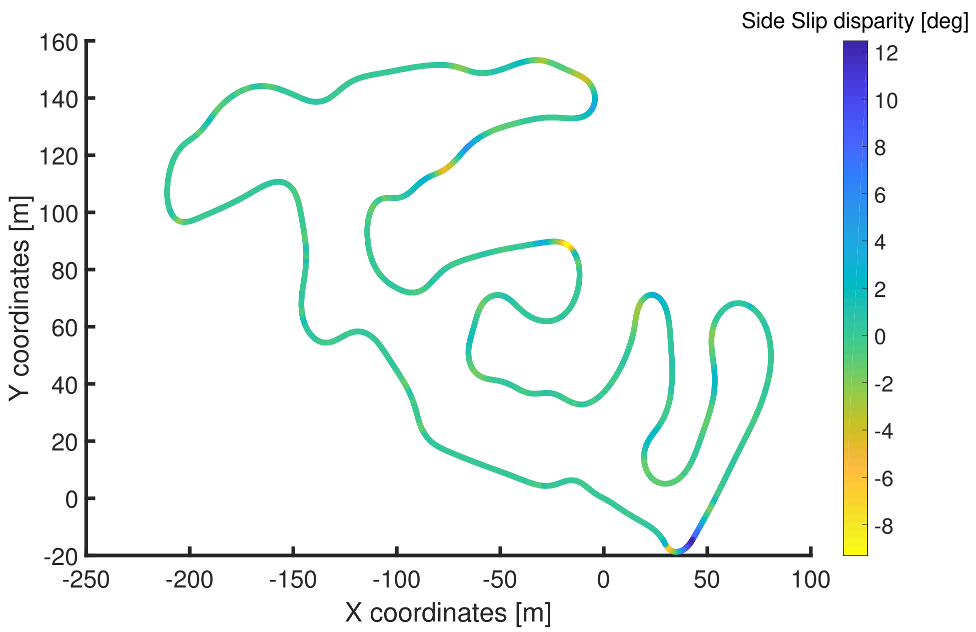

Figure 4.11: *Side slip angle disparity between the yaw–beta controller and the yaw controller.*

In Figure 4.12 the body side slip for both the yaw–beta and the yaw controller are shown. The yaw–beta controller achieved a body side slip standard deviation of 1.48°, whereas the same value for the yaw controller was 1.55°. The RMS body side slip of the yaw–beta controller and the yaw controller reached 1.48° and 1.56° respectively.

In addition to these parameters the lap time was also calculated for both the controllers. The lap time of the yaw–beta controller was 98.90 s while for the yaw controller it was 97.99 s.

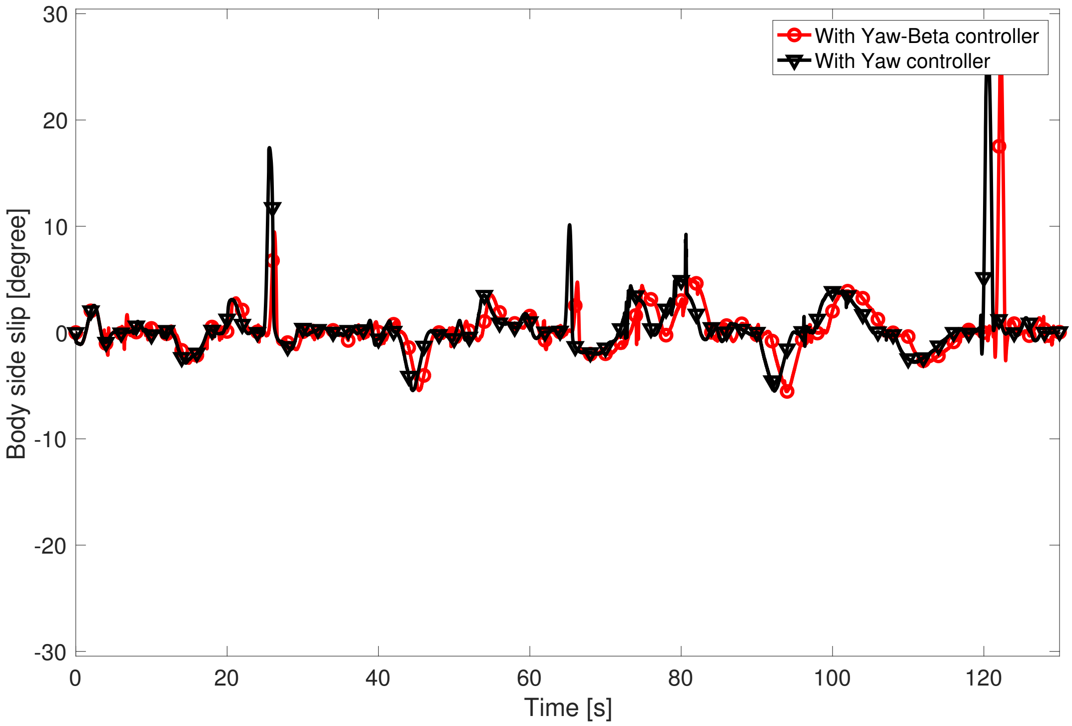

Figure 4.12: *Body side slip during track drive with yaw–beta controller and yaw controller.*

5 Discussion

This thesis presents a systematic approach for designing an MPC controller for yaw rate control and side slip angle control. It also describes the simulation environment, which was developed and used for simulating the controller action. This simulation environment is used to simulate the vehicle response for four different test scenarios. These tests are performed with two different MPC controllers: the yaw–beta controller and the yaw controller. These controllers differ from each other by the fact that the yaw–beta controller controls the yaw rate as well as the side slip angle where as the later only controls the yaw rate.

The first test scenario was chosen to be a step steer manoeuvre, as it is the most basic test to simulate the system response. The system response is measured in terms of rise time and overshoot. The rise time is the time required by the system output to reach 90% of the reference. Overshoot is achieved when the system output increases beyond the reference. Thus it can be reasoned that, minimising the rise time and overshoots can improve the performance of the controller. From the figure 4.1 and 4.2 it is evident that the rise time for the vehicle with the yaw–beta controller is higher than the the yaw controller. This is due to the fact that the yaw-beta controller tries to achieve a zero side slip angle which in turn limits the tire slip angles. This leads to a limited lateral performance and thus a slower system response. This means that the yaw–beta controller pushes the vehicle towards a stable state. Also, figure 4.3 supports this explanation. Figures 4.1 and 4.2 also show that the system output does not overshoot. This characteristic is the result of the predictive action of the controller.

The double lane change manoeuvre was simulated to observe the controller's ability to handle transient scenarios. Figure 4.4 shows that vehicle was able to perform the test with both the versions of the controller. In Figure 4.5 it is observed that for the yaw–beta controller the side slip peaks are lower which makes the vehicle more predictable in the cornering transient manoeuvre. These results are consistent with the outcome of the step steer manoeuvre, which shows that the yaw–beta controller will generate less side slip at the expense of slightly slower response time.

In order to push the vehicle to the limits of oversteering a sine with dwell test was simulated. Figures 4.6 and 4.7 compares the yaw rate for both the controller versions. As yaw–beta controller minimises the side slip angle deviation, it is easier for the vehicle to recover form an unstable state. This is also evident from recover time recorded from the results. Overall the results from this scenario were very similar for both the controller concepts. However, the changes seen do support that the yaw–beta controller generates less side slip.

For the previously mentioned test scenarios, the input was predefined. In order to test the control system in an open environment, a track drive simulation was performed on a racing map. This map is a combination of a variety of manoeuvres like chicanes, hair pins, constant radius turn, lane change, varying radius turns etc. This test also imposes a track boundary of 3 m width. Hence, this test simulates the overall performance of the controller system. A track curvature based longitudinal acceleration request and an aim point based yaw request is implemented. The vehicle performs a lap with the yaw–beta and the yaw controller. Disparity maps are plotted to evaluate the performance comparison with respect to the position on the map.

Figure 4.9 is used to conclude that the operating point for both the controllers is quite similar. Hence, the comparison results obtained are more robust and unbiased of velocity disparity. Also, the yaw–beta controller has a relatively lower corner entry speed and higher corner exit speed. As, the vehicle enters into a corner, the tire slip angle starts to build up. As the yaw–beta controller limits slide slip, it inherently limits the tire slip angles and hence slower corner entry. During corner exit, less time is required to recover from the corner since more traction is available, allowing a faster corner exit.

Figure 4.10 shows that the vehicle is not only fast but also precise. The lateral deviation values are less than 1 m, which suggests that the vehicle always stayed within the track boundary. The lower value of lateral deviation is credited to the aim point method used for reference generation.

Even though the lateral deviation showed small difference between the two controllers, Figure 4.11 displays a huge disparity range (-8°to 12°) for the side slip. These disparities occur at most demanding corners in the track. Such high values indicate that one or both vehicles entered a region of instability by exceeding the lateral friction limits. However, it is important to note that, despite such peaks in the side slip angle the vehicle with the yaw–beta controller manages to keep a lower side slip angle and stays on the track.

The discussion presented previously is used as a base to answer the research question posed by this thesis. The results from the step steer manoeuvre shows that using the yaw–beta controller reduces overshoots as compared to the yaw controller, but has a longer rise time. Also, the lap time results show that the yaw–beta controller is slower by 1 s as compared to the yaw controller on the FSG track. Thus, it can be said that, in the given simulation environment, the yaw controller performs faster than the yaw–beta controller, at the expense of being close to the instability limits. It is important to note here that this conclusion is solely based on the simulation results from virtual tests. As the simulation environment does not consider the effect of many variables and does not model all the non-linearities, the simulation results will not correspond to the actual results, if tested in the real vehicle. But these simulations are still valuable as they can be used to develop and verify the controller logic.

Also, it is uncertain how the choice of driver model might impact the results. Where the two systems differ is how they choose a steering angle for a given yaw-rate reference. Both systems are given the same longitudinal request, but perhaps a more optimal speed profile can be used once the information about lateral velocity is known.

In order to obtain a more conclusive answer to the research question, field testing is required. Hence, field testing of both the controller system is recommended to be done on an autonomous formula student vehicle. This testing will comprise of recreating the previously discussed test scenarios in real life and comparing the field test results to the simulation results. This comparison can be used to accurately determine the limitations of the given simulation environment.

6 Conclusion

The results of the simulation show that the performance of the yaw–beta controller is similar to the yaw controller. Thus, adding a side slip estimator does not show a significant improvement in the performance of the vehicle in the simulation environment. The performance of the vehicle refers to performance indices lap time, rise time, overshoot, positional deviation from path and body side slip mentioned in section 1.1. It is quite unreasonable to expect the simulation results to reflect the same results as during field testing as the simulation is limited in its capacity to predict the actual vehicle behaviour. This limitations can be transient behaviour, temperature dependency of tires, kinematic motion of the suspension, compliance in the system, wear etc. Although the limitations being known, it is quite challenging to model these limitations due to the complexity of the mathematics behind it.

Even though the results show small differences in between the two systems, they all point towards the initial hypothesis that the yaw–beta controller will lower the side slip of a vehicle in extreme scenarios. Lowering peak side slips could have a positive impact in vehicles due to less exposure to unstable driving events. What this thesis fails to conclude is the significance of this benefit in road vehicles.

The method of vehicle control adopted in this thesis can be tailored to be used in the passenger vehicles. Instead of using the control strategy to maximise performance, it can be adjusted to improve the safety of the passenger vehicle. To implement this method commercially, a perception system that identify objects with accuracy and an algorithm that can identify the stationary objects in the immediate environment will be required.

It can be concluded that the approach used in the thesis to control the vehicle produces a satisfactory result in the given simulation environment. Due to the limitations of the simulation environment, the potential of the controller can not be determined. Hence, to validate the true potential of the controller and to further improve the performance of the controller, real time testing would be required.

References

[1] H. Tokutake, Y. Sugimoto, and T. Shirakata, Real-time identification method of driver model with steering manipulation, *Vehicle System Dynamics* **51**, no. 1 2013, 109–121, 2013. DOI: 10.1080/00423114.2012.715175. eprint: https://doi.org/10.1080/00423114.2012.715175. [Online]. Available: https://doi.org/10.1080/00423114.2012.715175.

[2] S. "Akca and S. Ertugrul, "Ets fuzzy driver model for simultaneous longitudinal and lateral vehicle control
, *"International Journal of Automotive Technology"* **"15"**, no. "5" "Aug" "2014", "781–794", "Aug" "2014". DOI: "10.1007/s12239-014-0082-y". [Online]. Available: https://doi.org/10.1007/s12239-014-0082-y.

[3] T. P. Le, L. V. Dat, and I. Stiharu, "Application of neural networks to design the controller for autonomous vehicles by learning driver's behavior", *2013 International Conference on Control, Automation and Information Sciences (ICCAIS)*, Nov. 2013, pp. 1–6. DOI: 10.1109/ICCAIS.2013.6720520.

[4] M. Wasim, A. U. Awan, A. Kashif, M. M. Khan, and M. Abbasi, "Predictive control for improving vehicle handling and stability", *2015 9th International Conference on Electrical and Electronics Engineering (ELECO)*, Nov. 2015, pp. 879–884. DOI: 10.1109/ELECO.2015.7394581.

[5] B. Lacroix, Z. H. Liu, and P. Seers, "A comparison of two control methods for vehicle stability control by direct yaw moment", *Product Design and Manufacture*, ser. Applied Mechanics and Materials, vol. 120, Trans Tech Publications, Jan. 2012, pp. 203–217. DOI: 10.4028/www.scientific.net/AMM.120.203.

[6] M. K. Aripin, Yahaya Md Sam, Kumeresan A. Danapalasingam, Kemao Peng, N. Hamzah, and M. F. Ismail, A review of active yaw control system for vehicle handling and stability enhancement, *International Journal of Vehicular Technology* **2014**, no. 15 2014, 15, 2014. DOI: 10.1155/2014/437515. [Online]. Available: https://dx.doi.org/10.1155/2014/437515.

[7] S. Mammar and D. Koenig, Vehicle handling improvement by active steering, *Vehicle System Dynamics* **38**, no. 3 2002, 211–242, 2002. DOI: 10.1076/vesd.38.3.211.8288. eprint: http://www.tandfonline.com/doi/pdf/10.1076/vesd.38.3.211.8288. [Online]. Available: http://www.tandfonline.com/doi/abs/10.1076/vesd.38.3.211.8288.

[8] S. Ç. Balamili, İ. E. Köse, and G. Anlaç, Handling stability improvement through robust active front steering and active differential control, *Vehicle System Dynamics* **49**, no. 5 2011, 657–683, 2011. DOI: 10.1080/00423111003671900. eprint: https://doi.org/10.1080/00423111003671900. [Online]. Available: https://doi.org/10.1080/00423111003671900.

[9] X. Yang, Z. Wang, and W. Peng, Coordinated control of afs and dyc for vehicle handling and stability based on optimal guaranteed cost theory, *Vehicle System Dynamics* **47**, no. 1 2009, 57–79, 2009. DOI: 10.1080/00423110701882264. eprint: https://doi.org/10.1080/00423110701882264. [Online]. Available: https://doi.org/10.1080/00423110701882264.

[10] N. Tavan, M. Tavan, and R. Hosseini, An optimal integrated longitudinal and lateral dynamic controller development for vehicle path tracking, en, *Latin American Journal of Solids and Structures* **12** Jun. 2015, 1006–1023, Jun. 2015, ISSN: 1679-7825. [Online]. Available: `http://www.scielo.br/scielo.php?script=sci_arttext&pid=S1679-78252015000601006&nrm=iso`.

[11] M. Canale and L. Fagiano, Comparing rear wheel steering and rear active differential approaches to vehicle yaw control, *Vehicle System Dynamics* **48**, no. 5 2010, 529–546, 2010. DOI: `10.1080/00423110902919055`. eprint: `https://doi.org/10.1080/00423110902919055`. [Online]. Available: `https://doi.org/10.1080/00423110902919055`.

[12] W. Cho, J. Yoon, J. Kim, J. Hur, and K. Yi, An investigation into unified chassis control scheme for optimised vehicle stability and manoeuvrability, *Vehicle System Dynamics* **46**, no. sup1 2008, 87–105, 2008. DOI: `10.1080/00423110701882330`. eprint: `https://doi.org/10.1080/00423110701882330`. [Online]. Available: `https://doi.org/10.1080/00423110701882330`.

[13] L. Junwei and Y. Huafang, "Fuzzy logic applied to yaw moment control for vehicle stability", *2009 International Conference on Mechatronics and Automation*, Aug. 2009, pp. 386–390. DOI: `10.1109/ICMA.2009.5245096`.

[14] S. Zheng, H. Tang, Z. Han, and Y. Zhang, Controller design for vehicle stability enhancement, *Control Engineering Practice* **14**, no. 12 2006, 1413–1421, 2006, ISSN: 0967-0661. DOI: `https://doi.org/10.1016/j.conengprac.2005.10.005`. [Online]. Available: `http://www.sciencedirect.com/science/article/pii/S0967066105002406`.

[15] D. M. Bevly, J. Ryu, and J. C. Gerdes, Integrating ins sensors with gps measurements for continuous estimation of vehicle sideslip, roll, and tire cornering stiffness, *IEEE Transactions on Intelligent Transportation Systems* **7**, no. 4 Dec. 2006, 483–493, Dec. 2006, ISSN: 1524-9050. DOI: `10.1109/TITS.2006.883110`.

[16] J. Yi, J. Zhang, D. Song, and S. Jayasuriya, "Imu-based localization and slip estimation for skid-steered mobile robots", *2007 IEEE/RSJ International Conference on Intelligent Robots and Systems*, Oct. 2007, pp. 2845–2850. DOI: `10.1109/IROS.2007.4399477`.

[17] G. Reina, G. Ishigami, K. Nagatani, and K. Yoshida, "Vision-based estimation of slip angle for mobile robots and planetary rovers", *2008 IEEE International Conference on Robotics and Automation*, May 2008, pp. 486–491. DOI: `10.1109/ROBOT.2008.4543254`.

[18] A. Karlsson, Test procedures and evaluation tools for passenger vehicle dynamics 2014, 2014. [Online]. Available: `http://publications.lib.chalmers.se/records/fulltext/211557/211557.pdf`.

[19] P. Leischner, Proofs of the inscribed angle theorem 2010, 2010. [Online]. Available: `https://cermat.org/i2geo2010/downloads/files/I2GEO2010-Leischner.pdf`.

[20] H. B. Pacejka and E. Bakker, The magic formula tyre model, *Vehicle System Dynamics* **21**, no. sup001 1992, 1–18, 1992. DOI: `10.1080/00423119208969994`. eprint: `https://doi.org/10.1080/00423119208969994`. [Online]. Available: `https://doi.org/10.1080/00423119208969994`.

[21] G. J. Forkenbrock and P. L. Boyd, *Light vehicle esc performance test development*,